Supplementary Material for

Replay of cortical spiking sequences during human memory retrieval

Alex P. Vaz, John H. Wittig Jr., Sara K. Inati, Kareem A. Zaghloul*

*Corresponding author. Email: kareem.zaghloul@nih.gov

Published 6 March2020, *Science* **367**, 1131 (2020)
DOI: 10.1126/science.aba0672

This PDF file includes:

Supplementary Materials

Materials and Methods

Participants

6 participants (2 female; 34.8 ± 4.7 years) with drug resistant epilepsy underwent a surgical procedure in which platinum recording contacts (PMT Corporation, Chanhassen, MN) were implanted subdurally on the cortical surface as well as deep within the brain parenchyma (Supplementary Table S1). A subset of these participants (3 of 6) were included in a previous study (*25*). For research purposes, we placed one or two 96-channel microelectrode arrays (MEA; 4 x 4 mm, Cereplex I; Blackrock Microsystems, Inc., Salt Lake City, UT) in the anterior temporal lobe (ATL) of each participant in addition to the subdural grid (Fig. 1a,b) (*27*, *28*). MEAs were implanted only in participants with a presurgical evaluation indicating clear seizure localization in the temporal lobe. Hence, the implant site in the MTG was chosen to fall within the expected resection area. Each MEA was placed in an area of cortex that appeared normal both on the pre-operative MRI and on visual inspection. Across participants, MEAs were implanted 14.6 ± 3.7 mm away from the closest subdural electrode with any ictal or interictal activity identified by the clinical team. Four out of the six participants received a surgical resection which includes the tissue where the MEAs were implanted. One participant had evidence of focal cortical seizure activity and received a localized resection posterior to the MEA site. One participant did not have a sufficient number of seizures during the monitoring period to justify a subsequent resection. Neither participant experienced a change in seizure type or frequency following the procedure, or experienced any noted change in cognitive function. The NINDS Institutional Review Board (IRB) approved the research protocol, and we obtained informed consent from the participants explicitly for the placement of the MEAs and for all research components of this study.

Paired-associates memory task

Each participant performed a paired associates verbal memory task (*25*, *27*) (Fig. 2a, Fig. 3b). During the study period, participants were sequentially shown a list of word pairs (encoding period) and instructed to remember the novel associations between each pair of words. Later during testing, they were cued with one word from each pair selected at random (retrieval period), and were instructed to say the associated word into a microphone.

A single experimental session for each participant consisted of 25 lists, where each list contained six pairs of common nouns shown on the center of a laptop screen. The number of pairs in a list was kept constant for each participant. Words were chosen at random and without replacement from a pool of high-frequency nouns and were presented sequentially and appearing in capital letters at the center of the screen. In order to ensure that memory formation and retrieval were not directly adjacent in the task, study word pairs were separated from their corresponding retrieval cue by a minimum lag of two study or test items. During the study period (encoding), each word pair was preceded by an orientation stimulus (‘+’) that appeared on the screen for 250-300 ms followed by a blank interstimulus interval (ISI) between 500-750 ms. Word pairs were then presented stacked in the center of the screen for 4000 ms followed by a blank ISI of 1000 ms. Following the presentation of the list of word pairs, participants completed an arithmetic distractor task of the form A + B + C = ? for 20 seconds.

During the test period (retrieval), one word was randomly chosen from each of the presented pairs and presented in random order, and the participant was asked to recall the other word from the pair by vocalizing a response. Each cue word was preceded by an orientation stimulus (a row of question marks) that appeared on the screen for 250-300 ms followed by a blank ISI of 500-750 ms. Cue words were then presented on the screen for 4000 ms followed by a blank ISI of 1000 ms. Participants could vocalize their response any time during the recall period after cue presentation. We manually designated each recorded response as correct, intrusion, or pass. A response was designated as pass when no vocalization was made or when the participant vocalized the word 'pass'. During pass trials where no vocalization was present, we assigned a response time by randomly drawing from the distribution of correct response times during that experimental session. We defined all intrusion and pass trials as incorrect trials. A single experimental session contained 150 total word pairs. Each participant completed between 1-3 sessions (2.2 ± 0.3 per participant).

Intracranial EEG (iEEG) recordings

We collected intracranial EEG (iEEG) data from a total of 716 subdural and depth recording contacts (119 ± 16.0 per participant). Subdural contacts were arranged in both grid and strip configurations with a contact radius of 1.5 mm and inter-contact spacing of 10 mm. These contacts could lie along medial temporal lobe (MTL) structures including the parahippocampal gyrus and entorhinal cortex. We designated an electrode as residing in the MTL if its placement was medial to the collateral sulcus, excluding the uncus. We analyzed data from 48 subdural contacts (8.0 ± 0.5 per participant) in brain regions applicable to our study. These included MTL designated electrodes and electrodes placed in the lateral temporal association cortex overlying the MEAs. We analyzed these areas given previous evidence demonstrating the role of interactions between the MTL and the association cortex in memory retrieval (*25*), and because we were interested in examining the relation between cortical iEEG and micro-scale local field potentials and spiking activity captured in the MEAs.

Contact localization was accomplished by co-registering the post-op CTs with the post-op MRIs using both FSL Brain Extraction Tool (BET) and FLIRT software packages and mapped to both MNI and Talairach space using an indirect stereotactic technique and OsiriX Imaging Software DICOM viewer package. The resulting contact locations were subsequently projected to the cortical surface of a Montreal Neurological Institute N27 standard brain (*31*). Pre-operative MRIs were used when post-operative MR images were not available. We identified the location of each MEA on a surface reconstruction created using each participant's pre-operative T1 weighted MRI (FreeSurfer, http://surfer.nmr.mgh.harvard.edu). Individual participant reconstructions were co-registered with a standard template brain, and the locations of each participant's MEA were visualized on the template brain (Fig. 1b).

Depending on the amplifier and the discretion of the clinical team, iEEG signals were sampled at 1000 or 2000 Hz. For clinical visual inspection of the recording, signals were referenced to a common contact placed subcutaneously, on the scalp, or on the mastoid process. The recorded raw iEEG signals used for analyses were referenced to the system hardware reference, which was set by the recording amplifier (Nihon Kohden, Irvine CA) as the average of two intracranial electrode channels. We re-referenced these raw signals using bipolar referencing in order to mitigate any effects of volume conduction or any biases introduced by the system hardware reference (*25*). All recorded traces were resampled at 1000 Hz, and a fourth order 2 Hz stopband Butterworth notch filter was applied at 60 Hz to eliminate electrical line noise.

We quantified spectral power and phase by convolving iEEG signals with complex valued Morlet wavelets (wavelet number 6). We extracted 4 s of data from every encoding and retrieval trial, beginning with the presentation of the words on the screen, for our analyses. In all trials, we included a 2000 ms buffer on both sides of the clipped data. To generate corresponding power spectrograms, we calculated spectral power using 40 linearly spaced wavelets between 5 and 200 Hz. We then squared and log-transformed the continuous-time wavelet transform to generate a continuous measure of instantaneous power. To account for changes in power across experimental sessions, we z-scored power values separately for each frequency and for each session using the mean and SD of all respective values for that session.

Ripple detection

We detected ripple events as reported previously (*25*). We first bandpass filtered the iEEG signal in the ripple band (80-120 Hz) using a second order Butterworth filter, and then applied a Hilbert transform to extract the instantaneous amplitude within that band. We selected events where the Hilbert envelope exceeded 2 standard deviations above the mean amplitude of the filtered traces. Only events that were at least 25 ms in duration and had a maximum amplitude greater than 3 standard deviations were retained as ripples for analysis. We joined adjacent ripples that were separated by less than 15 ms. We identified every ripple that satisfied these criteria in every electrode contact, and assigned each such identified ripple a start time index and an end time index. The difference between them defined the duration of each ripple.

Importantly, high frequency activity can be associated with epileptiform activity in addition to cognitive processes. Therefore we implemented several measures to provide the most conservative sampling of non-pathological signals possible. We implemented a previously reported automated trial and electrode rejection procedure based on excessive kurtosis or variance of iEEG signals (*25*, *27*). We calculated and sorted the mean iEEG voltage across all trials, and divided the distribution into quartiles. We identified trial outliers by setting a threshold, Q3+w*(Q3-Q1), where Q1 and Q3 are the mean voltage boundaries of the first and third quartiles, respectively. We empirically determined the weight w to be 2.3. We excluded all trials with mean voltage that exceeded this threshold. The average percent removed across all sessions in each participant due to either system-level noise or transient epileptiform activity was 4.6 ± 3.4% of all trials.

In addition, system level line noise, eye-blink artifacts, sharp transients, and interictal epileptiform discharges (IEDs) can be mistakenly characterized as ripples after high pass filtering. We therefore implemented a previously reported automated event-level artifact rejection (*22*, *25*). We calculated a z-score for every iEEG time point based on the gradient (first derivative) and amplitude after applying a 250 Hz high pass filter (for identification of epileptogenic spikes). Any time point that exceeded a z-score of 5 with either gradient or high frequency amplitude was marked as artifactual, and 125 ms before and after each identified time point was also classified as an artifact. We visually confirmed that the above methodology reliably identified IEDs and high frequency oscillations associated with IEDs (ripple on spike waveforms) (*25*). We excluded all IEDs and all such pathologic ripples from our analyses. The remaining ripples that we retain for our analyses therefore occur without an associated IED and are more likely to be physiologic.

Identification of single units

We identified single units as reported previously (*27*, *28*). Briefly, microelectrodes were arranged in a 10 × 10 grid with each electrode spaced 400 μm apart and extending 1.5 mm into the cortical surface (1.0 mm for one participant). Post-operative paraffin blocks of the resected tissue demonstrated that the electrodes

extended approximately halfway into the 3 mm-thick gray matter. We digitally recorded microelectrode signals at 30 kHz using a Cerebus acquisition system (Blackrock Microsystems), with 16-bit precision and a range of ± 8 mV. To extract neuronal spiking activity, we re-referenced each electrode's signal offline by subtracting the mean signal of all the electrodes in the MEA, and then used a second order Butterworth filter to bandpass the signal between 0.3 to 3kHz. We extracted micro-scale local field potential (LFP) signals in the same manner, but instead used a 500 Hz low pass filter. Using a spike-sorting software package (Plexon Offline Sorter, Dallas, TX, USA), we identified spike waveforms by manually setting a negative or positive voltage threshold depending on the direction of putative action potentials. The voltage threshold was set to include noise signals used in calculating unit isolation quality (see below). Waveforms (duration, 1.067 ms; 32 samples per waveform) that crossed the voltage threshold were stored for spike sorting. Spike clusters were manually identified by viewing the first two principal components, and the difference in peak-to-trough voltage (voltage versus time) of the waveforms. We manually drew a boundary around clusters of waveforms that were differentiable from noise throughout the experimental session (Fig. S2). In this manner, we identified a total of 989 putative single units across all sessions (average of 72.2 ± 20.7 units per participant). The average spike rate across all units was 2.5 ± 0.6 Hz (Fig. S20).

Due to variability in the signal quality across recordings and the subjective nature of spike sorting, we quantified the quality of each unit by calculating an isolation score and signal to noise ratio (SNR). The isolation score quantifies the distance between the spike and noise clusters in a 32-dimensional space, where each dimension corresponds to a sample in the spike waveform. The spike cluster consisted of all waveforms that were classified as belonging to that unit, and the noise cluster consisted of all waveforms that crossed the threshold that were not classified as belonging to any unit. The isolation score is normalized to be between 0 and 1, and serves as a measure to compare the isolation quality of all units across all experimental sessions and participants. Across participants, the mean isolation score for all units was 0.93 ± 0.1.

In addition to isolation quality, we computed the SNR for each unit using the following equation:

$$SNR = \frac{V_{peak} - V_{trough}}{Noise * C}$$

where V_{peak} and V_{trough} are the maximum and minimum voltage values of the mean waveform, and C is a scaling factor (set as 5). To obtain *Noise*, we subtracted the mean waveform from each individual waveform for each identified unit, concatenated these waveform residuals, and then computed the standard deviation of this long vector. Therefore, the noise term quantifies the within-unit variability in waveform shape. Across participants, the mean SNR for all units was 1.71 ± 0.12.

Identification of burst events and sequences

In order to identify burst events, we calculated the instantaneous population spike rate by convolving a gaussian kernel (σ = 25 ms) across the spike rasters for each unit. We obtained an average spike rate over each trial for each unit, and then averaged across all units to obtain an average population spike rate for each trial. We used the distribution of trial averaged spike rates to determine the mean and standard deviation of the population spike rate for each experimental session. Within each session, we then defined the burst event threshold as three standard deviations above the mean of the distribution of trial averaged spike rates. We identified burst events as an event exceeding this threshold for at least 25 ms. We assigned the time point with the highest population spike rate within each burst event as the temporal index of that burst event, and we defined the burst event window as the time period ±75 ms from this index. In

order to avoid extracting sequences from overlapping burst events that likely indicated the same event, we removed any event that was within 150 ms of another by removing the event with the lower spiking rate. Events that extended outside of the trial window boundaries (eg. after start of vocalization) were excluded in order to retain only trial relevant spiking activity.

We performed all analyses on sequence replay based on the spiking sequences detected during these burst events (*9–12*). Detected bursts of spiking activity were tightly correlated with detected ripple oscillations at both the macro- and micro-scale (Fig. 1c-e; Fig. S3-5). However, this relation was not absolute, suggesting that many spike events are associated with ripples that do not exceed the threshold for detection, and that the ability to detect a ripple using these parameters is highly influenced by the level of spiking activity (Fig. S4,5). Our data also suggest that the relation between detected ripples and bursts of spiking activity is more robust at the micro-scale.

Across participants, burst events had a mean unit spike rate of 6.2 ± 1.8 Hz, involved 39.9 ± 6.3 % of units identified per session, and had a mean inter-event interval of 579 ± 71 ms (Fig. S21-23). Units with lower spike rates were more likely to fire within burst events (correlation between average spike rate per unit and fraction of spikes within burst events: $r = -0.35 \pm 0.06$, $t(5) = -5.60$, $p = .003$; Fig. S24). Additionally, because we observed changes in spike rates between correct and incorrect trials, we calculated the Fano factor to quantify any change in the variance of spiking activity (*32*). We calculated the Fano factor of each unit as the across-trial variance of the spike rate divided by the corresponding mean spike rate (*28*), and we averaged across all units to generate a single value for each trial type in each participant (Fig. 3g, Fig. S19). We quantified the duration of each sequence in our dataset as the time difference between the first and last spike of that sequence. The durations of sequences were similar between encoding and retrieval for both correct (reported in main text) and incorrect trials (encoding: 108.5 ± 10.4 ms; retrieval: 108.7 ± 10.5 ms; $t(5) = -0.244$, $p = 0.817$).

Once burst events had been identified, we extracted sequences from the units that fired during each event. We identified these sequences by determining the temporal order of maximal firing rate of each unit within the burst event time window (Fig. S6). We calculated the rates of each unit with the same gaussian kernel above and assigned each unit a position within the extracted sequence based on when its maximum firing rate occurred within the burst event window. We based all calculations of sequence similarity between pairs of burst events on the sequences of maximal firing in each burst event identified in this manner.

For visualization purposes, but not for analyses of sequence similarity, we also generated a template sequence that captures the average temporal ordering of single unit firing in repeated bursts within an individual encoding trial (Fig. 2c, Fig. 3b, Fig. 4b, and Fig. S9). This template sequence allows for the visualization of the average order of firing for neurons in a single trial, even though each individual burst within that trial typically has a different specific order. To generate this template sequence, we examined spiking activity during the encoding period of each trial and cross-correlated the single trial spike trains from each unit with all other units. For N active neurons in a trial, this creates $N(N-1)/2$ possible combinations. For each cross-correlation, we separately summed the counts 250 ms before and 250 ms after zero to determine which unit within each pair fired first on average. In this manner, we could assign each unit a position in a template sequence based on how many other units it fired before on average. Importantly, we only generated this template sequence using the encoding spike trains, and we used this template sequence to visualize the emergence of matching sequences over time during retrieval.

To determine the difference in replay content between sequences within burst events that were coupled to MTL ripples versus those that were uncoupled, we first determined the temporal relationship between MTL

ripples and cortical replay. Based on our findings of significant cortical replay up to approximately 175 ms after the onset of MTL ripples (Fig. 4c), we classified a burst event as coupled if its center index fell within 175 ms of the start index of an MTL ripple on any channel. All other burst events were then classified as uncoupled, and the average replay values during the last second of the retrieval period were calculated separately for each category (Fig. 4d).

Quantification of sequence similarity

We quantified sequence similarity using the matching index (*12*). For a given sequence of length N, a total of N(N-1)/2 pairs can be assessed between neurons occurring in different positions within the sequence. For a second sequence that is to be matched to the first, we define *m* as the number of pairs of neurons that fire in the same order as in the first sequence, and *n* as the number of pairs of neurons that fire in the opposite order. The matching index (MI) is then defined as:

$$MI = (m - n) \,/\, (m + n)$$

MI is bounded between -1 and 1, indicating exactly reverse and forward replay, respectively, of the second sequence of interest relative to the original sequence. We determined the significance for how similar a given sequence pair is by randomly rearranging the temporal positions of units in each sequence 1000 times, calculating the MI for each permutation, and comparing the true MI to the shuffled distribution (*12*).

Because matching indices varied significantly across experimental sessions and participants (Fig. S8,S9), we z-scored MI values within each session in order to make these values comparable across participants. We generated a distribution of MI values that arise when comparing all pairwise across-trial combinations of encoding sequences within each experimental session in each participant. This distribution of MI values computed for each session represents a null distribution of similarity between sequences that would arise by chance. We used the mean and standard deviation of this across-trial distribution to z-score subsequent measures of MI. Hence, to confirm that sequences during the encoding period were specific for each trial, we averaged the pairwise MI between all sequences within each trial, and z-scored this value using the mean and standard deviation of the across-trial distribution (Fig. 2e). Similarly, to compare the sequence similarity between burst events during retrieval to those during encoding (Fig. 3,4), we averaged the matching index between each retrieval event to all encoding events from the same trial, and we z-scored each average retrieval value to the mean and standard deviation of all values computed in this manner for each session in each participant. However, while we used z-scored MI values for all main analyses, we also replicated the main findings of the study using the raw MI values for both encoding and retrieval (Fig. S25).

Each retrieval trial contained several replay values existing at discrete points in time. To examine the changes in replay over time across trials and participants (Fig. 3d), we computed a running mean of the z-scored MI values in each trial using a 1000 ms sliding window (1 ms steps) and smoothed the resulting curves with a gaussian kernel (σ = 50 ms). We averaged this continuous time measure of sequence similarity across all correct and incorrect trials, and compared these average traces between participants. We employed a non-parametric clustering based procedure to identify time epochs that exhibited a significant difference in sequence replay between correct and incorrect trials (*33*). The clustering procedure identifies contiguous temporal epochs exhibiting significant differences between trial types with the null hypothesis that across participants, each epoch showed no difference for correct versus incorrect trials. For each time epoch, we computed the true t-statistic and *p*-value across participants between correct and incorrect trials. We then randomly permuted the participant-specific averages (correct vs incorrect), which

in practice translates to randomly reversing the sign of the difference within each participant and recomputing the mean difference across participants. For n participants, this results in an empiric distribution of 2^n possible mean differences that are all equally probable under the null hypothesis. We generated the empiric distribution from 1000 permutations for every epoch and calculated t-statistics for each of the permuted epochs. The p-value for each individual epoch in the true case, however, does not take into account the multiple comparisons that are made in time (across epochs).

To correct for multiple comparisons across epochs, we identified clusters containing epochs that were adjacent in time that exhibited a significant difference between trial types (where in each epoch, $p < .05$). For each cluster of significant epochs identified in the true and permuted cases, we defined a cluster statistic as the sum of the t-statistics within that temporal cluster. We retained the maximum cluster statistic during each of the 1000 permutations to create a distribution of maximum cluster statistics. We assigned p-values to each identified cluster of the true data by comparing its cluster statistic to the distribution of maximum cluster statistics from the permuted cases. Clusters were determined to be significant if their p-value calculated in this manner was less than .05.

We used a similar cluster-based approach to determine whether MTL triggered replay exhibited significantly greater sequence similarity than would be expected by chance. In this case, to analyze the smaller timescale of MTL triggered replay (Fig. 4c), we used a 200 ms sliding window and σ = 25 ms gaussian smoothing kernel to generate a continuous time measure of sequence similarity. We then averaged this continuous time measure across all correct trials and compared these traces to those generated after temporally jittering MTL ripples in a circular fashion to random values between -1000 ms and 1000 ms of the original indices. We employed the non-parametric clustering based procedure described above to compare the true continuous time measure of MTL-triggered replay to the temporally jittered data.

To confirm the presence of memory-specific replay of neural activity, we implemented a previously reported shuffling procedure (*25*) to compare replay values during correct trials to replay computed after shuffling trial labels (Fig. 3e,f). First, we shuffled the encoding-retrieval trial pairs for all correct and incorrect trials (Fig. 3e). In this manner, for N trials in a given session, the sequences for an individual retrieval trial were compared to all other non-matching encoding trials (for a total of N-1 comparisons for each trial). We computed the average shuffled value across all trials, and then compared this average to the average of the true encoding-retrieval replay values in each participant (Fig. 3e). We then performed two additional shuffling procedures. We shuffled all encoding-retrieval trial pairs using only correct trials, and we also shuffled the correct encoding-retrieval trial pairs by simply swapping the trial labels for all adjacent correct retrieval trials (Fig. 3f). If sequence replay reflects a behaviorally independent convergence of sequences over time as opposed to memory specific replay, then replay calculated using shuffled retrieval periods should be identical to that observed using the original correct trials. In all cases, the true unshuffled mean level of replay was significantly greater than the average replay in each shuffled condition, demonstrating that sequence replay is specific for each retrieved memory.

Given previous rodent literature showing that replay of sequences occurs during awake rest periods (*10*, *11*), we were also motivated to investigate the presence of any such neural activity during the paired associates task. We hypothesized that sequence replay during rest periods could preferentially replay previous successfully encoded memories. We identified all sequences in two separate rest periods: the intertrial intervals between successive retrieval trials during the retrieval portion of the task and the math distractor task between the encoding and retrieval blocks of each list (Fig. S17). We identified all sequences during a given rest period and then compared them to all previous encoding trials within the

same session block (6 word pairs per block). We therefore generated an average replay value of the rest period sequences compared to the encoding sequences that were later remembered (correct) versus those that were forgotten or incorrectly remembered (incorrect). In this manner, each set of rest period sequences was assigned a separate average replay value of previous correct versus incorrect encoding trials, and these values were averaged across trials and participants as conducted for all other analyses. We found that sequences within either rest period did not preferentially replay previous correct encoding periods compared to incorrect encoding periods (Fig. S17), suggesting that replay of spiking sequences occurs specifically following the test probe during correct retrieval trials.

To confirm that any similarity observed between sequences of spiking activity was related to the temporal sequence of unit firing rather than due to the identity of the neurons involved, we calculated the similarity in unit identity between burst events (Fig. S7). For a given session with N units, any given burst event can be represented as a vector of length N consisting of ones and zeros based on whether or not a unit fired during that event. We then calculated unit identity similarity between two burst events as the cosine similarity between the respective binary vectors. We additionally used the Jaccard index and found similar results (Fig. S7).

We additionally performed several control analyses to validate our metrics of sequence replay. First, we replicated our replay analysis within individual participants (Fig. S11). We also replicated our analysis using rank-order correlation (*10*, *11*) to calculate sequence similarity instead of the matching index, and we reproduced the same analyses by using nonparametric signed rank tests (Fig. S12). Next, because metrics of sequence similarity such as the matching index can only be calculated on units that are common to both sequences under comparison, it is possible that changes in the number of common units between sequence pairs could affect sequence similarity calculations. We therefore fixed the mean number of common units for encoding-retrieval pairs within each session to the mean number of common units for the correct trials (N). This was performed by randomly selecting a subset of common units of size N for each encoding-retrieval sequence comparison in the incorrect trials, and sequence comparisons with less than N common units were not included. This procedure was averaged over 1000 permutations in order to account for random selection of units. When the average number of matching units was fixed per session, we replicated the results where correct trials exhibited significantly greater sequence replay compared to incorrect trials (Fig. S13). Finally, we also demonstrated that sequence replay differences were not due to changes in burst rates or ripple rates (Fig. S14,S15).

Given previous findings of reinstatement of spiking activity during memory retrieval (*27*), we also quantified replay separately for unit identity and spike rate (Fig. S26). We found that the encoding-retrieval similarity of the identity of active units was not significantly different between correct and incorrect trials. However, spike rate similarity was significantly greater in correct trials when considering changes over the whole task window (Fig. S26). Further, because spiking characteristics varied significantly across participants in general and within burst events (Fig. S20-S22), we confirmed that sequence replay and spike rate similarity between encoding and retrieval were not correlated with the overall percentage of spikes within burst events for each participant (Fig. S27).

Supplementary Figures

Fig. S1

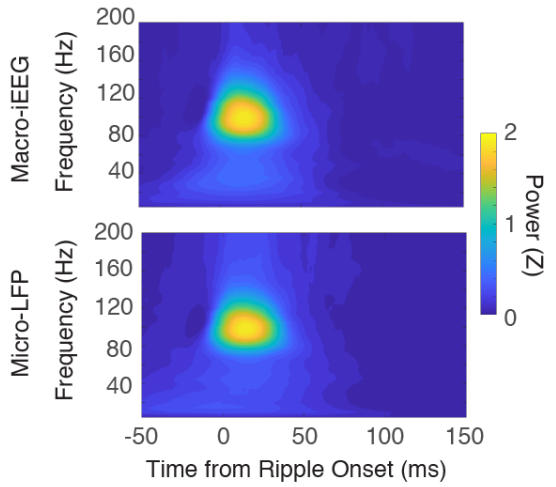

Both Macro-iEEG and micro-LFP ripples are band limited to 80-120 Hz. Average ripple triggered spectrograms for the macro-scale and micro-scale ripples detected in the middle temporal gyrus of the anterior temporal lobe. t = 0 indicates start index of detected ripple oscillation. Warmer colors indicate higher spectral power.

Fig. S2

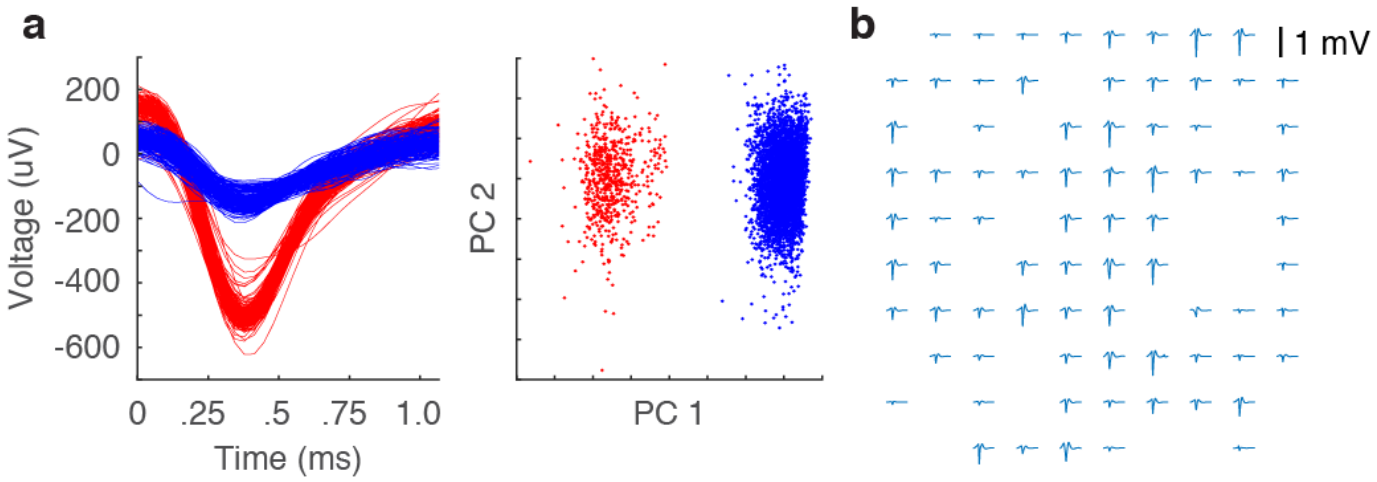

Example unit waveforms and cluster separation. a, Waveforms from two example sorted units (red and blue respectively) detected on the same MEA channel (left) with the associated PCA cluster separation (right) (*27*, *28*). **b**, Spatial arrangement and average waveforms of detected units on the 96 channel MEA.

Fig. S3

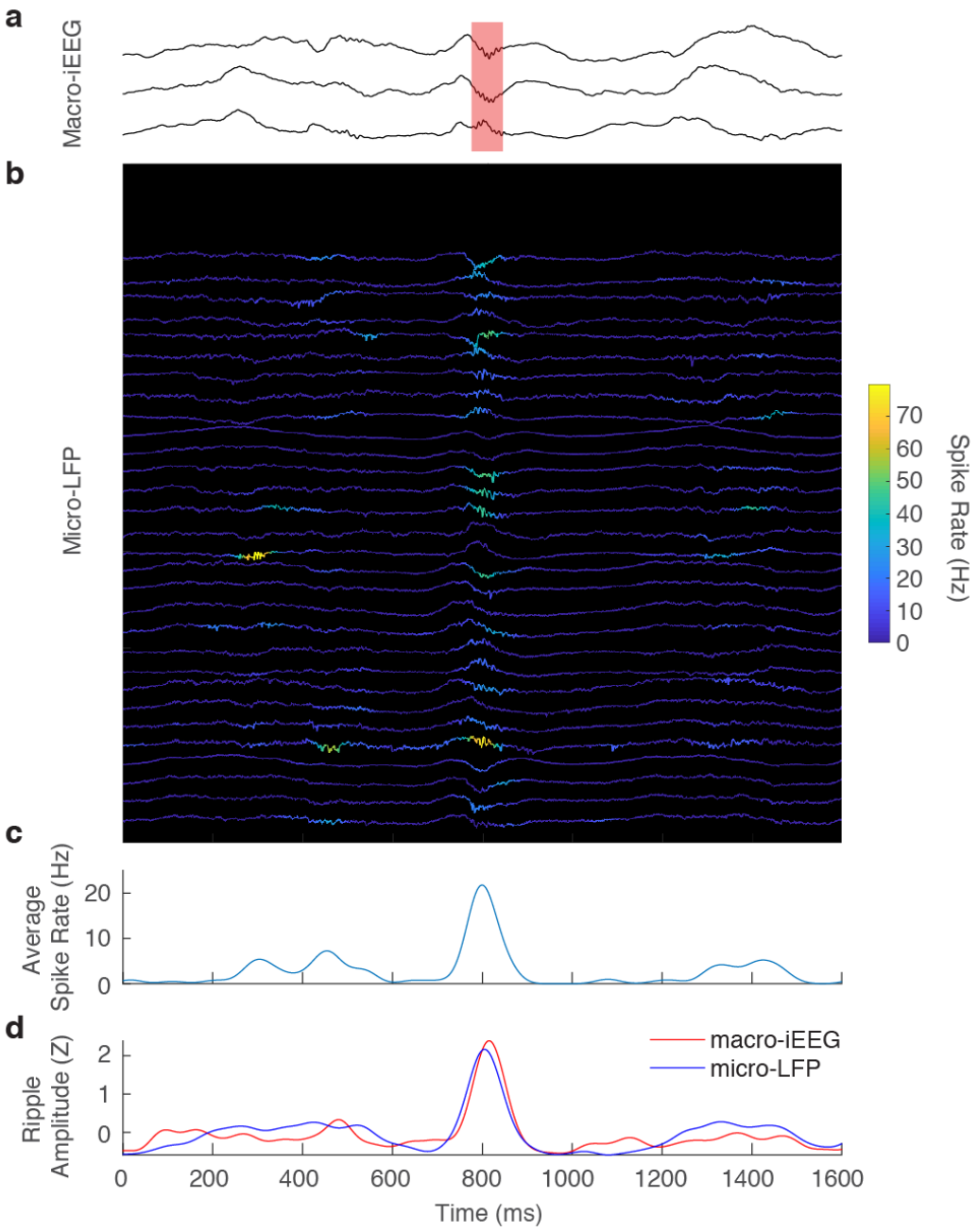

Micro-LFP ripples reflect local spiking activity and ripple band amplitude. a, Ripple oscillations detected in the cortical macro-iEEG. **b**, Corresponding ripple activity in the micro-LFP with the instantaneous spike rate of single units identified on that channel indicated by the color of the trace. Warmer colors indicate higher spike rates. Each ripple in the macro-iEEG was accompanied by a burst of spikes at the micro-scale. **c**, Average spike rate across all single units in this burst. **d**, Average ripple band amplitude (80-120 Hz) in both macro-iEEG (red) and micro-LFP (blue).

Fig. S4

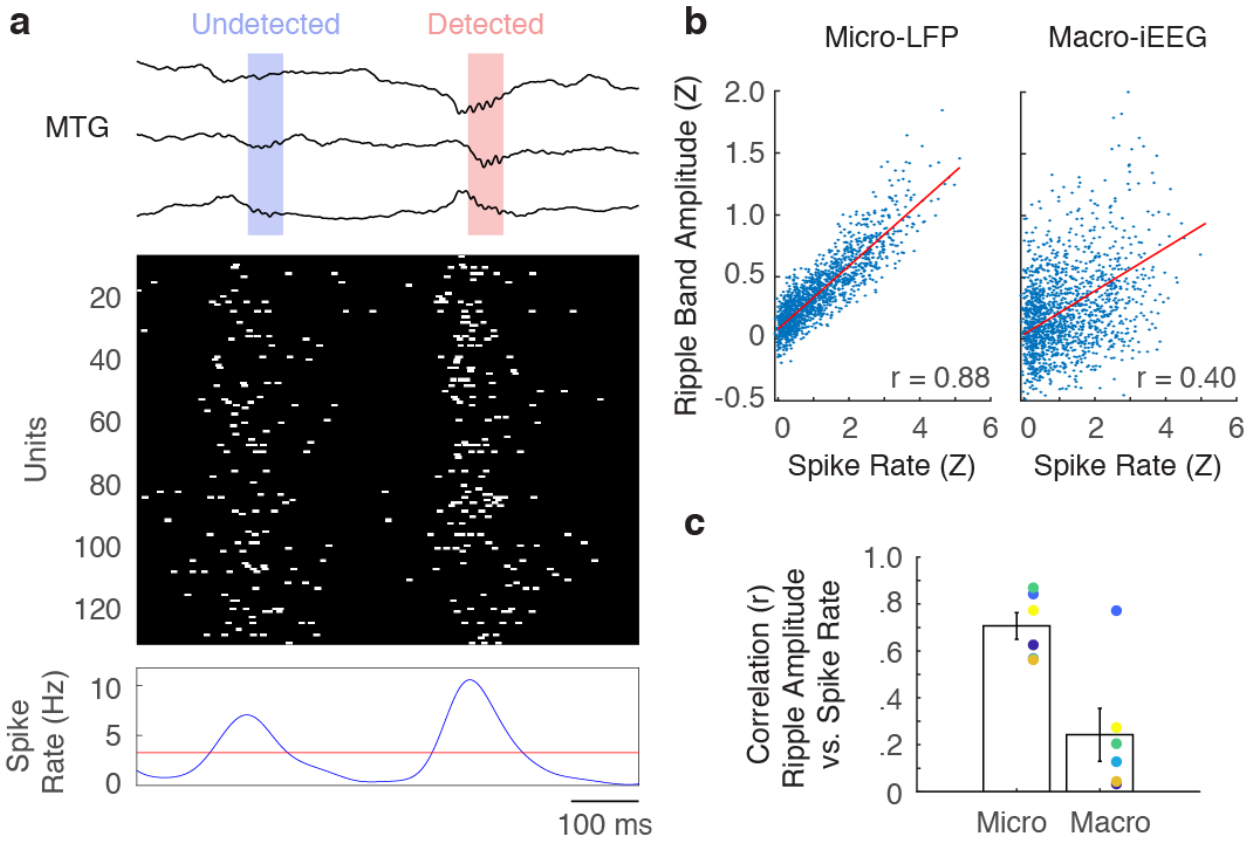

Relationship between spiking activity and ripple detection. a, Two representative burst events with variable ripple detection. Macro-iEEG signals (top) with detected ripples highlighted in red and putative ripples that were not detected highlighted in blue. Spike raster for all units in this recording session during the two events (middle). Instantaneous spike rates are shown below the raster in blue with the burst event threshold for that session shown in red (bottom). We defined a burst event as coupled to a cortical ripple if the ripple indices fell within 50 ms of the center of the burst event. Across participants, 82.4 ± 7.7% of all burst events were coupled to a micro-LFP ripple, and 13.2 ± 3.2% of burst events were coupled to a macro-iEEG ripple. Likewise, 40.3 ± 8.7% of all micro-LFP ripples and 40.6 ± 8.9% of macro-iEEG ripples were coupled to a burst event. **b**, Example session in a single participant demonstrating correlation between the average z-scored spike rate of each burst event and the average z-scored ripple band amplitude (80-120 Hz) across all electrodes. Each blue point is a detected burst event within that session, and the red line indicates the linear regression through all points. **c**, Across participant data of correlations between average population spike rate and average ripple band amplitude during all detected burst events. Each colored dot represents one participant. We found that this correlation between burst event spike rate and ripple band amplitude was consistently greater than chance in both the micro-LFP and macro-iEEG across participants (micro correlation = 0.71 ± 0.06, n = 6, signed rank test, p = 0.031; macro correlation = 0.24 ± 0.11, p = 0.031).

Fig. S5

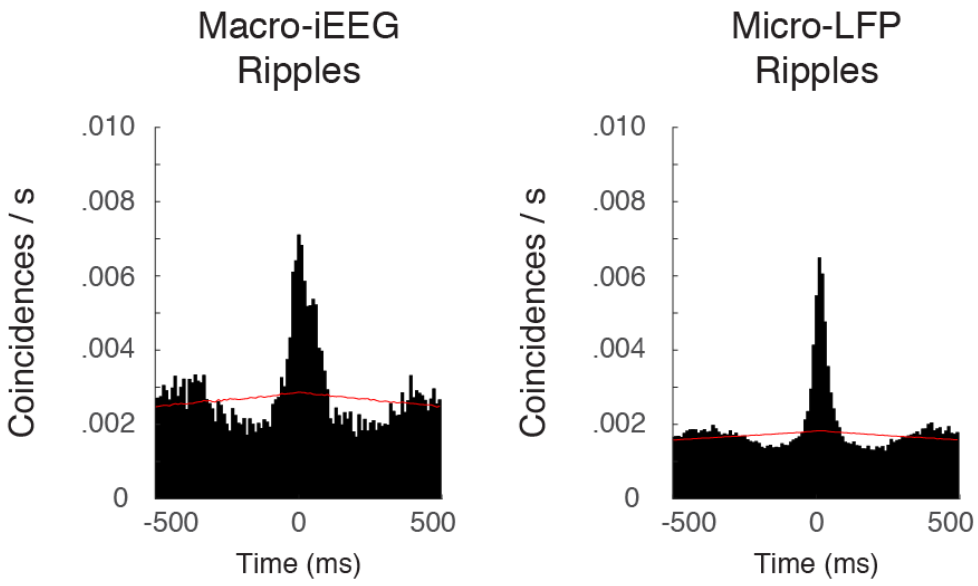

Temporal association of macro-iEEG and micro-LFP ripples with burst events. Cross-correlograms of detected ripples with detected spike burst events for macro-iEEG ripples (left) and micro-LFP ripples (right). 10 ms bins are used in all cases, and the first index of each ripple was used when calculating cross-correlations. Red lines indicate the shift predictors generated by cross-correlating after shuffling trial order. Synchronization was determined by calculating the ratio of cross correlation area to baseline area in a ±50 ms window, thereby synchronization = 1 indicates chance level (*25*). All participants exhibited synchronization that was greater than chance for both macro-iEEG and micro-LFP ripples (macro-iEEG ripple synchronization = 2.74 +/- 1.10, n = 6, signed rank test, p = 0.031; micro-LFP ripple synchronization = 3.29 +/- 1.26, p = 0.031).

Fig. S6

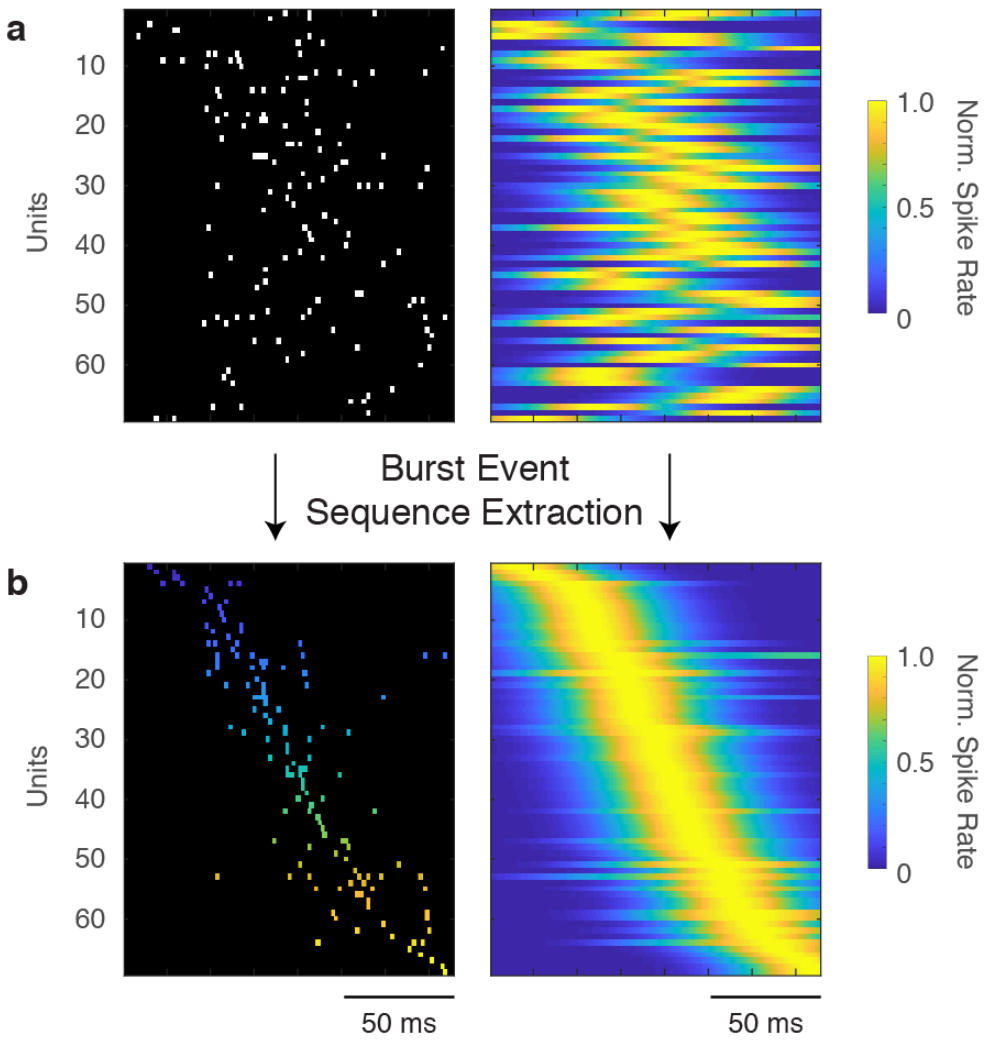

Example of sequence extraction from an individual burst event. a, An example of a raw burst event (left) is shown with instantaneous normalized spike rates for each unit (right). **b**, Same units after reordering (left) based on the temporal positions of the corresponding spike rates of each unit within that burst event (right). Colors for units in raster (left) indicate the extracted temporal order with cooler and warmer colors representing earlier and later in the sequence respectively. We determined the duration of each burst event using the time difference between the first and last spike.

Fig. S7

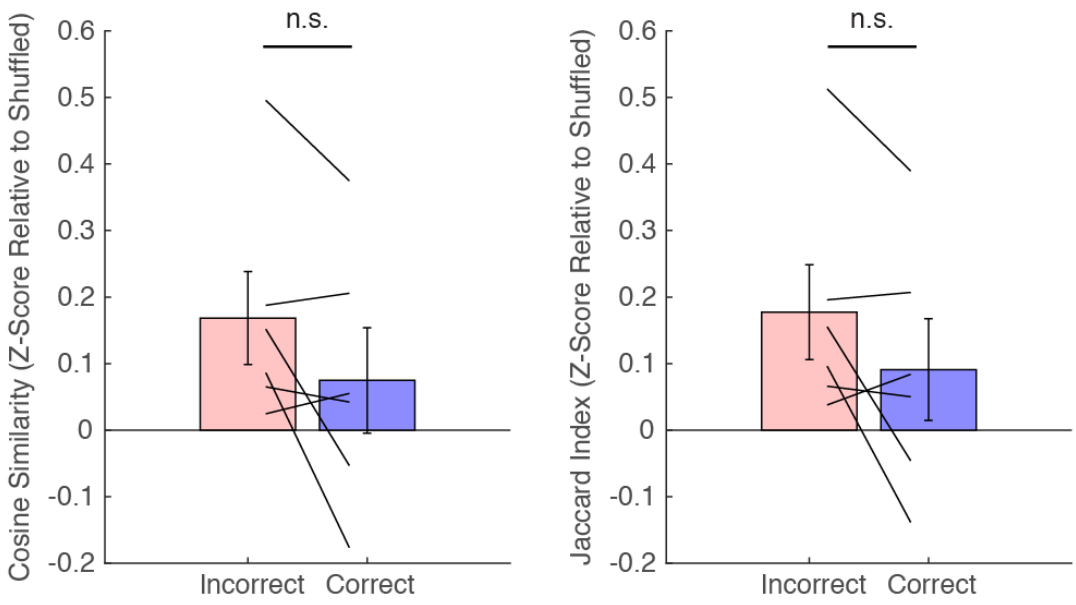

Unit identity similarity between burst events is not significantly changed during encoding. We quantified the extent to which any pair of burst events involved activity of the same units, independent of the specific temporal order with which the units fired. Correct trials did not demonstrate higher within-trial compared to across-trial similarity of unit identity during bursting events, as determined by cosine similarity (left) and Jaccard index (right; $p > 0.05$). These calculations are analogous to the sequence similarity measurements in Fig. 2e, and suggest that the specific temporal order of unit firing, rather than just the identity of the units that are active, is important for successful memory encoding.

Fig. S8

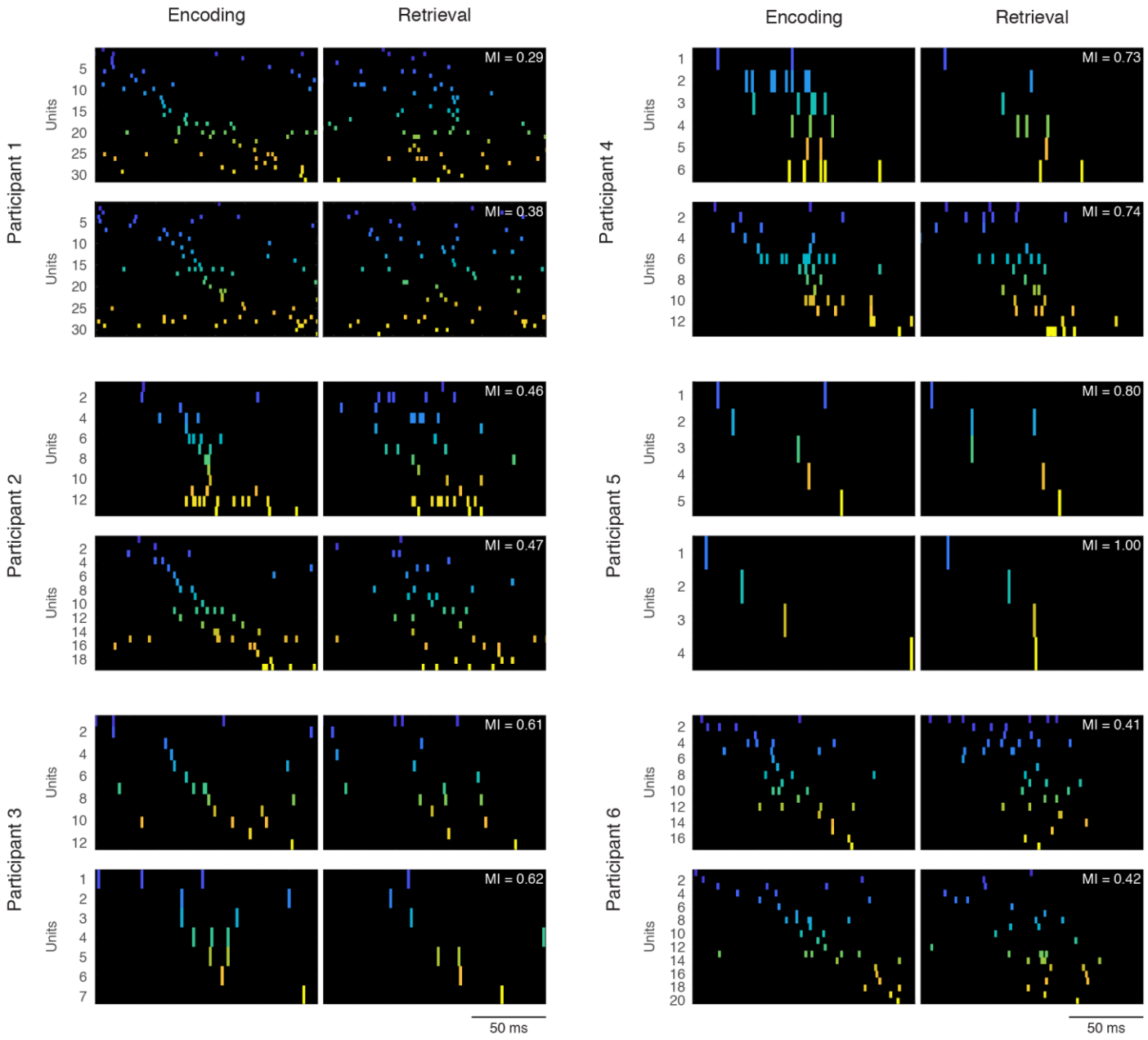

Individual examples of sequence replay for each participant. For each participant, two example replay events are shown from separate correct trials (top and bottom respectively). In each example, the spike raster from the encoding period is shown on the left and the corresponding retrieval period is shown on the right. Colors represent the temporal ordering during the encoding sequence of that trial with cooler and warmer colors representing earlier and later in the sequence respectively. The sequence similarity for each encoding-retrieval pair is indicated in the inset, and all replay events shown are significant ($p < 0.05$).

Fig. S9

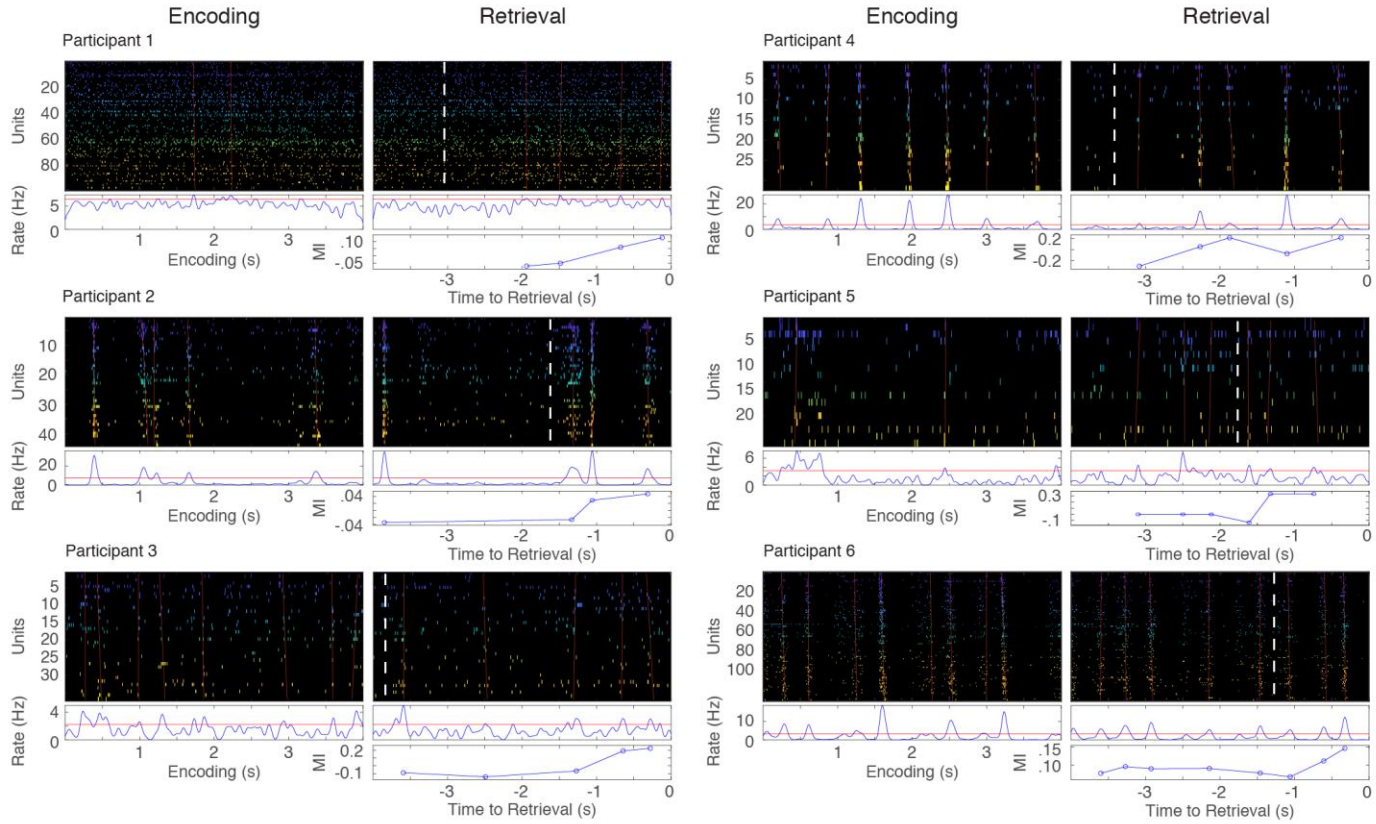

Single trial examples of correct encoding and retrieval for each participant. For each example trial in each participant, spike rasters are shown for both encoding (left) and retrieval (right). Colors represent the average temporal ordering during encoding with cooler and warmer colors representing earlier and later in the sequence respectively. White dashed line indicates the time of test probe presentation. Red lines indicate the linear regression through the maximum spike rate times of all units within each burst event. Instantaneous spike rates are shown below each raster (blue) with the burst event threshold for that session (red). The average sequence similarity of each retrieval burst event to all encoding events for the trial is shown below each retrieval raster.

Fig. S10

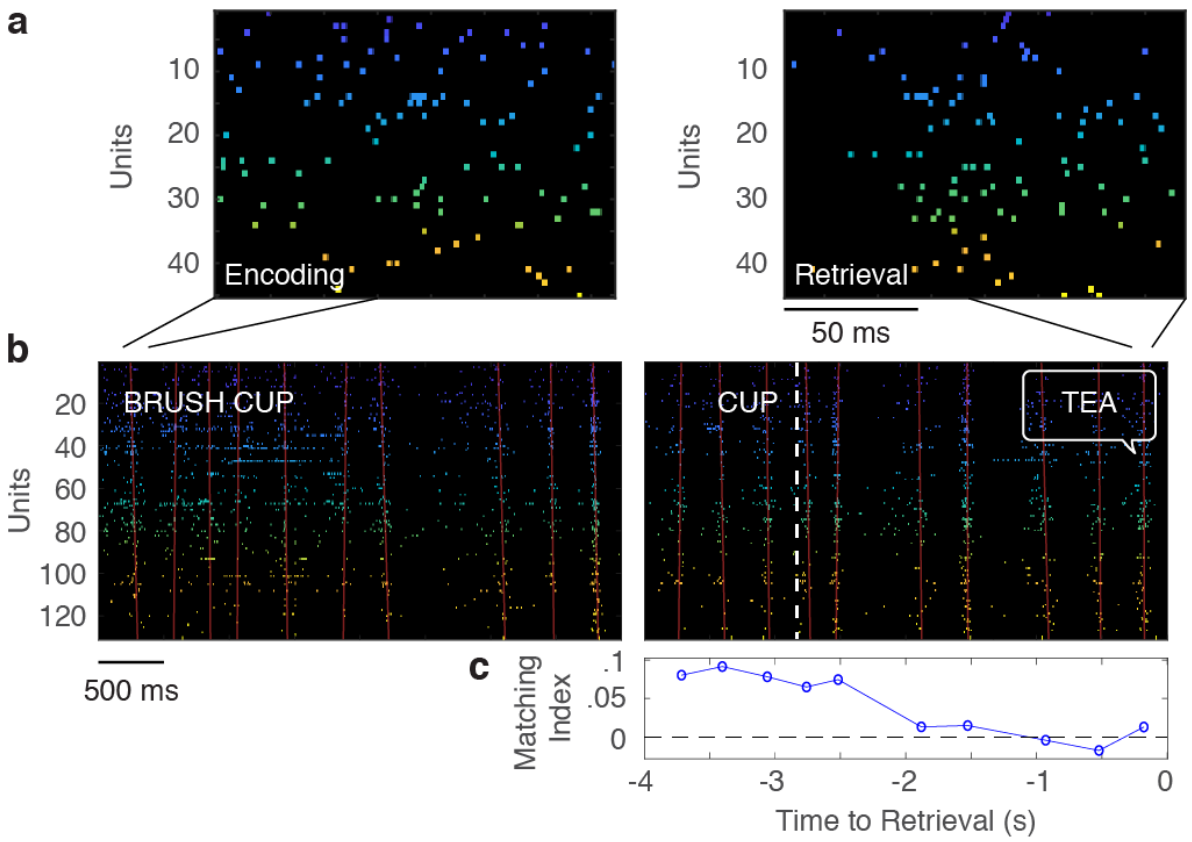

Incorrect trials do not display increased sequence replay during retrieval. a, Example sequence replay event during incorrect memory retrieval. Matching Index = -0.03 (p = 0.401) for this encoding-retrieval sequence pair. Colors represent the average temporal ordering during encoding with cooler and warmer colors representing earlier and later in the sequence respectively. **b**, Encoding (left) and retrieval (right) rasters of the corresponding trial in (a) during the paired associates task. Inset text indicates the study pair to be memorized (BRUSH CUP), the test probe (CUP), and the verbalized response (TEA). White dashed line indicates the time of test probe presentation. Red lines indicate the linear regression through the maximum spike rate times of all units within each burst event. **c**, Average sequence similarity of each retrieval burst event to all encoding events for the trial shown in (b).

Fig. S11

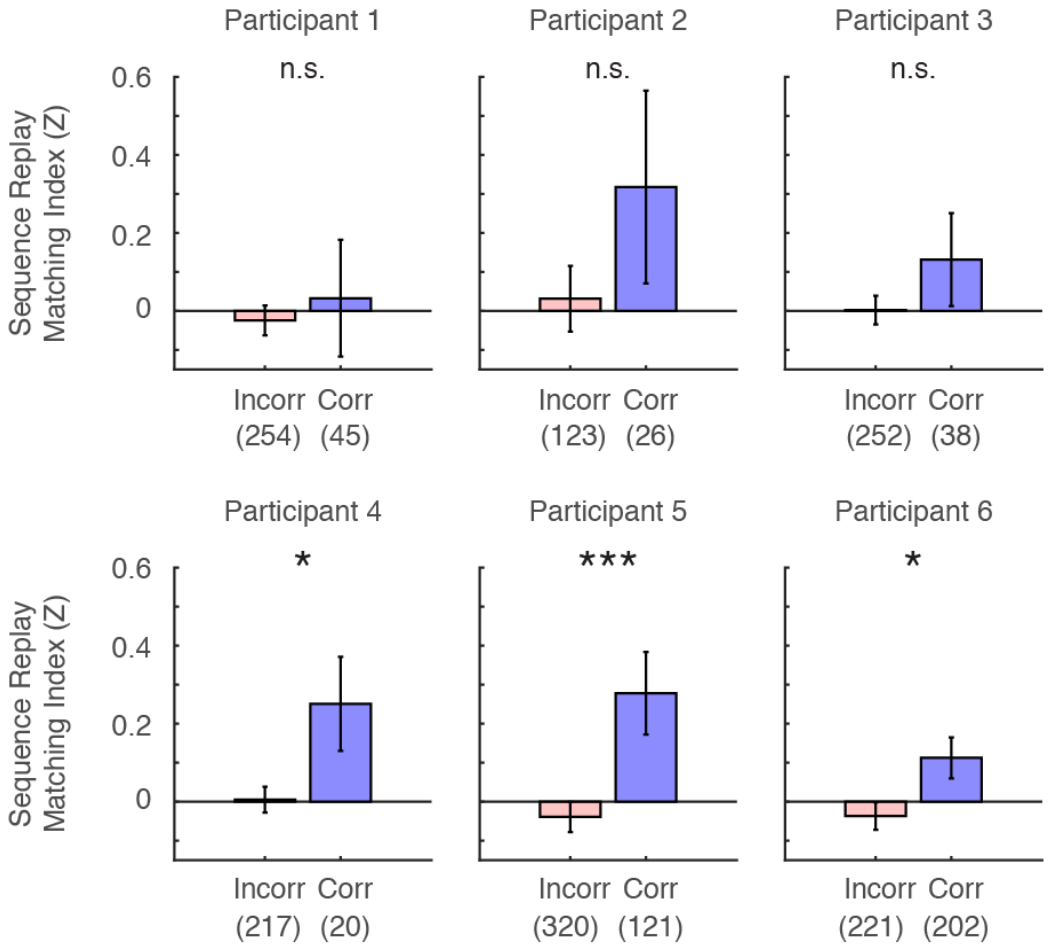

Sequence replay results reproduced within each participant. Average sequence replay values across all trials for each participant are shown for incorrect and correct retrieval trials. Total trial counts across all recording sessions are shown for each condition below each bar plot. Bars represent the SEM across all trials for that condition. All participants exhibited an average replay value for correct trials that was greater than for incorrect trials. Significance for individual participants was determined by two-sample t-test (*p < 0.05, ***p < 0.001).

Fig. S12

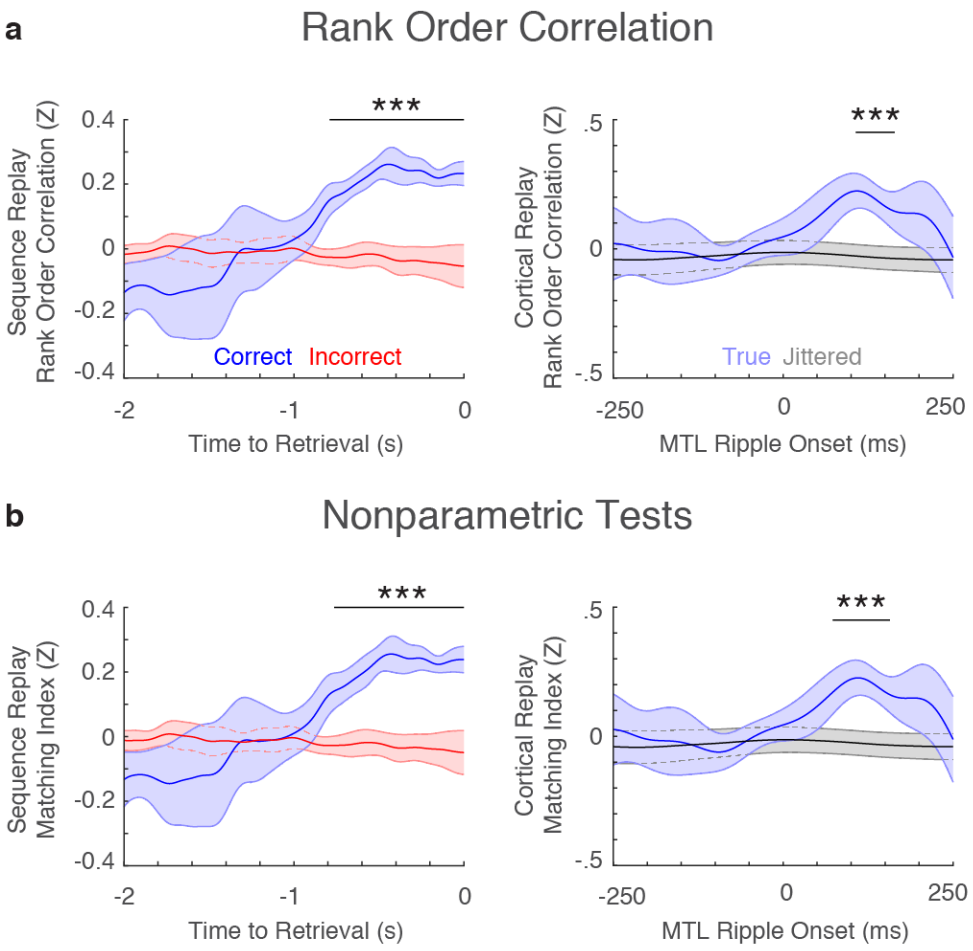

Replication of sequence replay results with alternative metrics of sequence similarity and nonparametric statistical tests. a, Replication of results with rank-order correlation. Sequence replay results during memory retrieval (left) and triggered to MTL ripples during retrieval (right) are preserved when using rank-order correlation (*10*, *11*) to calculate sequence similarity as opposed to matching index (*$p < 0.001$, permutation test). Bars indicate SEM across all participants. **b**, Replication of results using a signed-rank test to compare the matching index between conditions. Correct retrieval demonstrated significantly increased sequence similarity compared to incorrect retrieval with signed rank test as the preliminary statistical test before cluster correction for multiple comparisons (***$p < 0.001$, permutation test).

Fig. S13

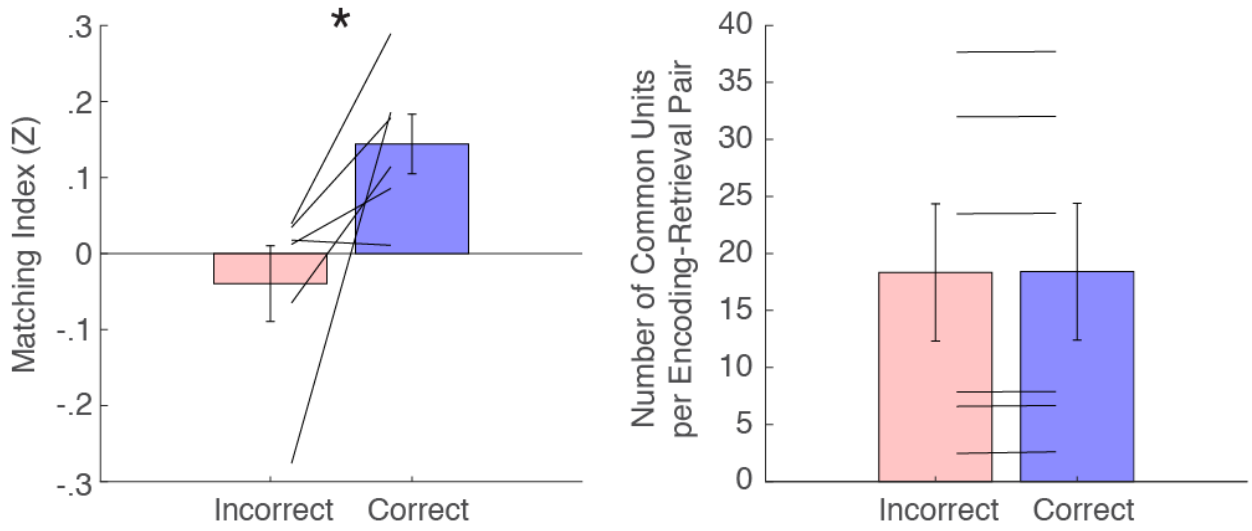

Replication of sequence replay results after fixing the average number of units common to both sequences during similarity calculations. The number of units that are active in each sequence can possibly affect the calculation of MI that quantifies the similarity between pairs of sequences. Because, on average, spike rates decreased during correct trials, we performed an additional analysis in which we re-calculated sequence similarity in incorrect trials by fixing the number of common units per encoding-retrieval pair to the average value in the correct trials. Increased sequence replay in correct trials compared to incorrect trials was maintained (left; $t(5) = 2.77$, $p = 0.039$) even when fixing the number of units used to calculate the similarity between pairs of sequences in this fashion (right). This analysis complements the finding that sequence replay was not correlated with the number of units used to calculate sequence similarity.

Fig. S14

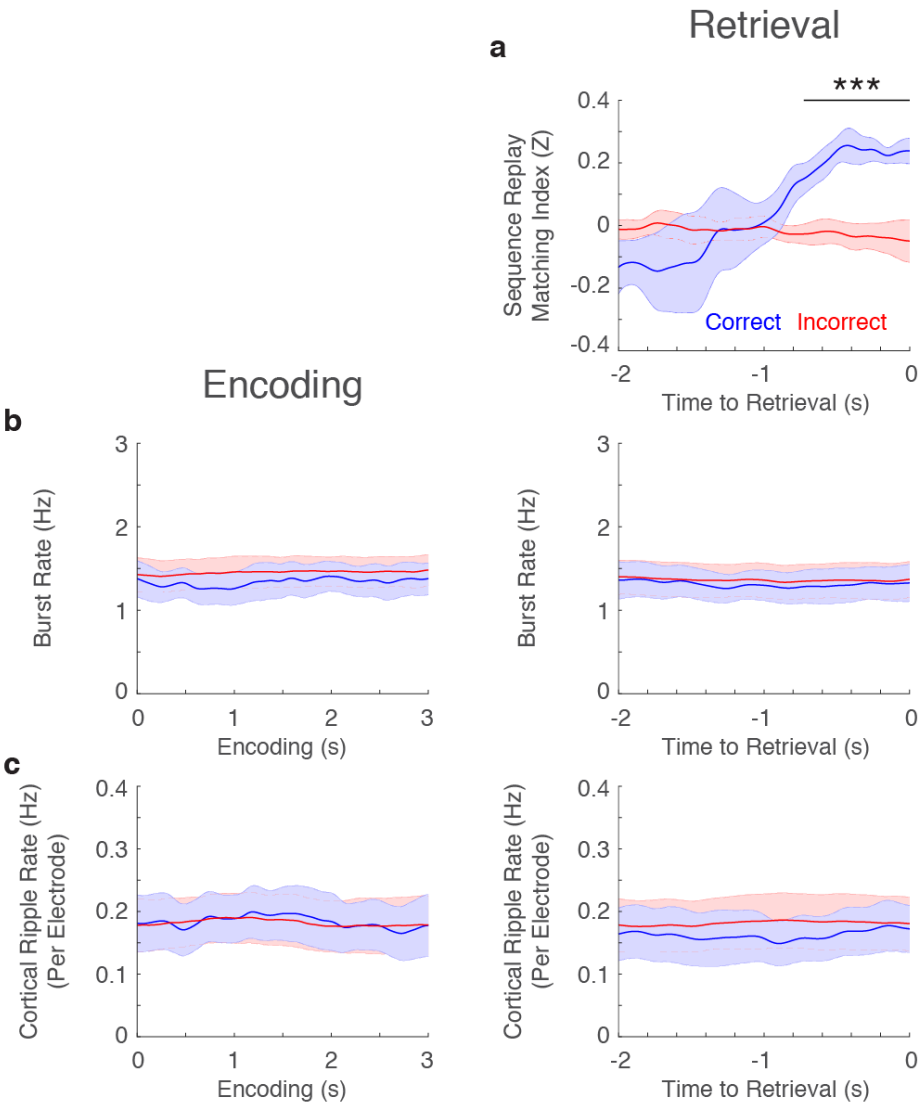

Cortical burst event and ripple rates do not significantly change during successful encoding and retrieval. a, Average similarity of retrieval sequences to encoding sequences across all participants during memory retrieval. Bars indicate SEM across all participants. Correct retrieval demonstrated significantly increased sequence similarity compared to incorrect retrieval (***$p < 0.001$, permutation test). **b**, Average burst event rate across all participants for encoding (left) and retrieval (right). **c**, Average macro-iEEG ripple rate per electrode across all participants for encoding and retrieval. No significantly different epochs were identified for correct versus incorrect conditions.

Fig. S15

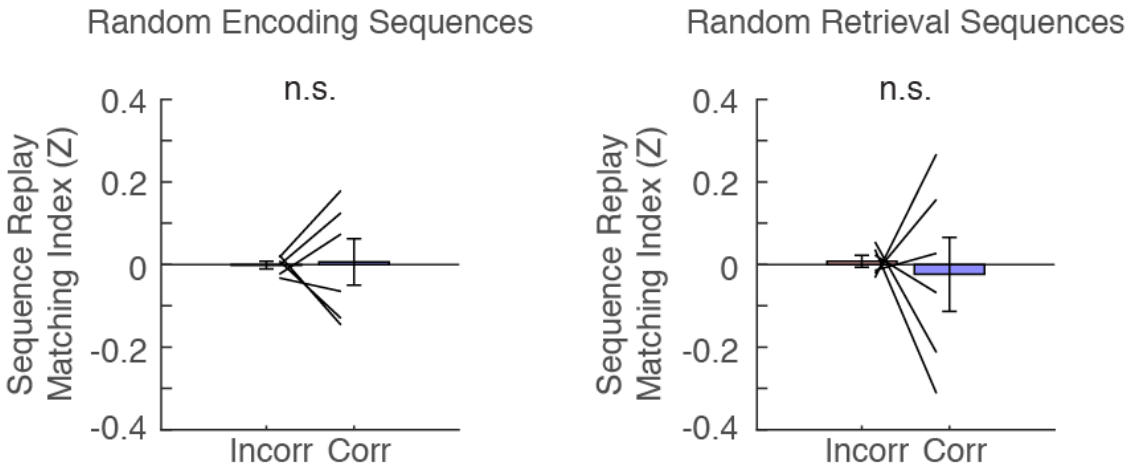

Changes in burst event frequency during encoding or retrieval do not account for increased sequence replay for correct trials. We performed an additional control analysis where we replaced all sequences with uniform length, randomized sequences in either all encoding or all retrieval trials. If changes in burst event rate during correct encoding or retrieval were confounding factors that led to measurement of increased sequence replay, then comparisons to random sequences should also display increased sequence similarity. However, we observed that comparisons of the true encoding to random retrieval sequences (left) and random encoding sequences to true retrieval sequences (right) both yielded no significant difference between correct and incorrect trials across participants. These results indicate that burst event rate dynamics cannot account for measured increased sequence replay levels during correct trials, and that the temporal ordering of the sequences leads to measurement of replay.

Fig. S16

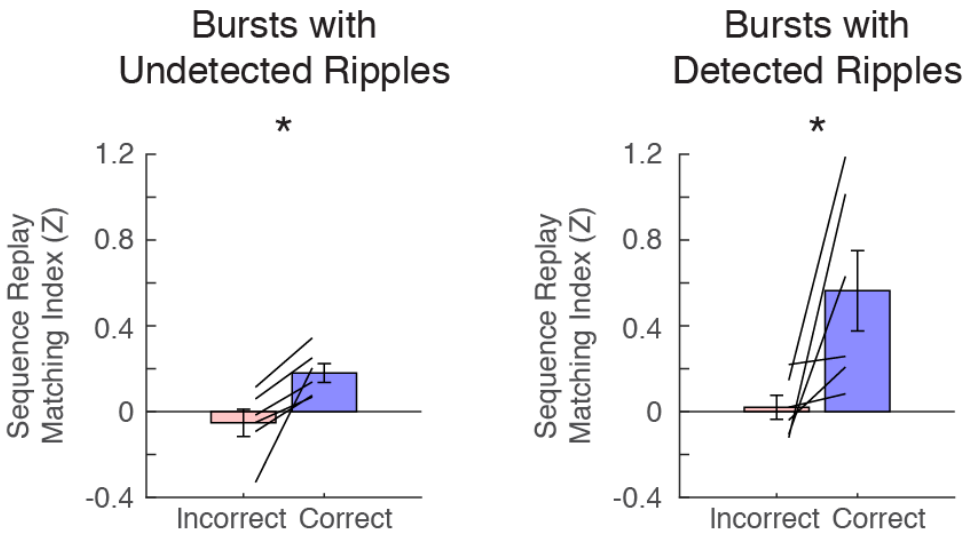

Replication of replay results after separating burst events based on detection of simultaneous ripples in the cortical macro-iEEG. We defined a burst event as one that is associated with a detected macro-iEEG ripple if any ripple event was within 50 ms of the center index of the burst event. Correct memory retrieval exhibited significantly increased sequence replay compared to incorrect trials when considering burst events when an associated macro-iEEG ripple was not detected (left) and when an associated macro-iEEG ripple was detected (right). Each line indicates a single participant and bars indicate SEM across all participants. In correct trials, bursts associated with ripples did not display significantly higher sequence replay than the bursts with no associated ripples ($n = 6$, $t(5) = 1.90$, $p = 0.115$).

Fig. S17

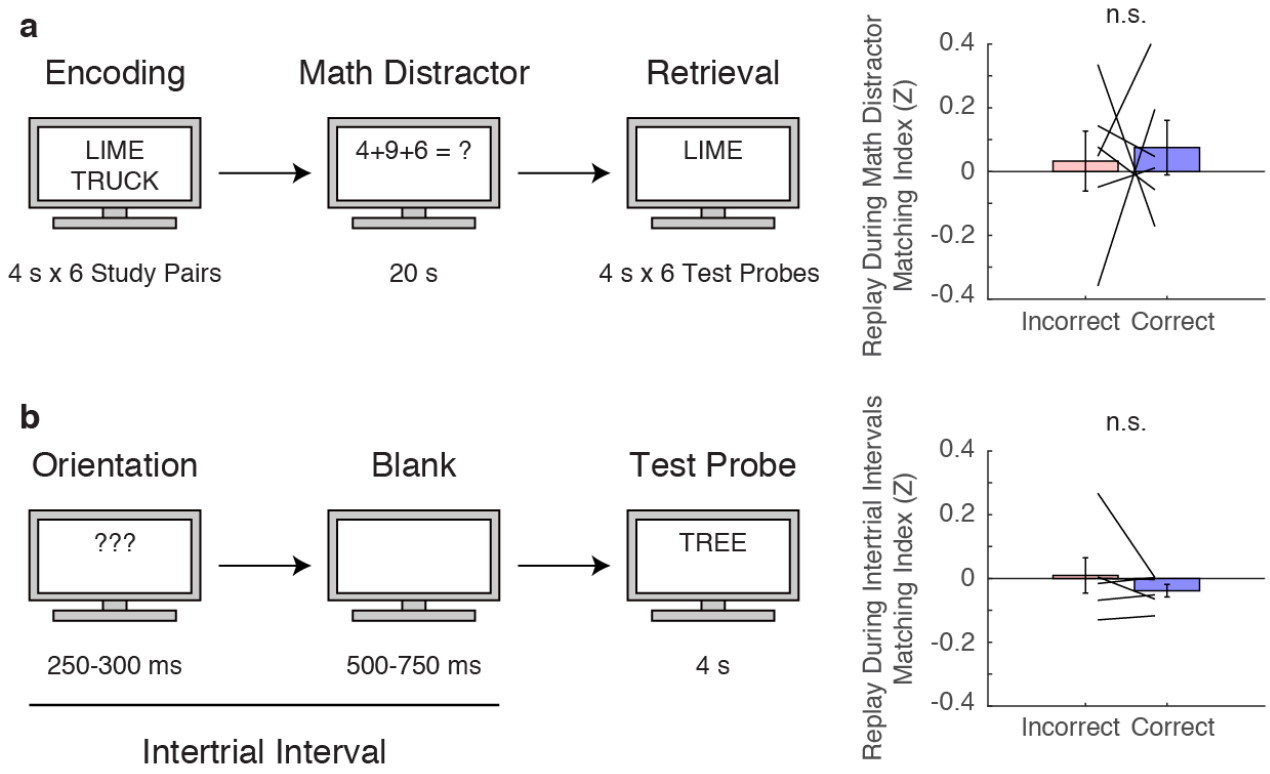

Analysis of potential sequence replay during rest periods in the paired associates task. a, Participants completed an arithmetic distractor task of the form A + B + C = ? for 20 seconds between the encoding and retrieval blocks (left). Average similarity of rest period sequences to correct and incorrect encoding trials from the same word list consisting of 6 pairs (right). Each line indicates a single participant and bars indicate SEM across all participants. Sequences detected during this period did not preferentially replay correct encoding trials. **b**, Intertrial intervals during the retrieval period (left). These intervals were composed of an orientation cue (???) followed by a blank screen before the test probe presentation. Sequences detected during this period also did not preferentially replay correct encoding trials (right), suggesting that replay of spiking sequences occurs specifically during memory retrieval that begins following the test probe in correct retrieval trials.

Fig. S18

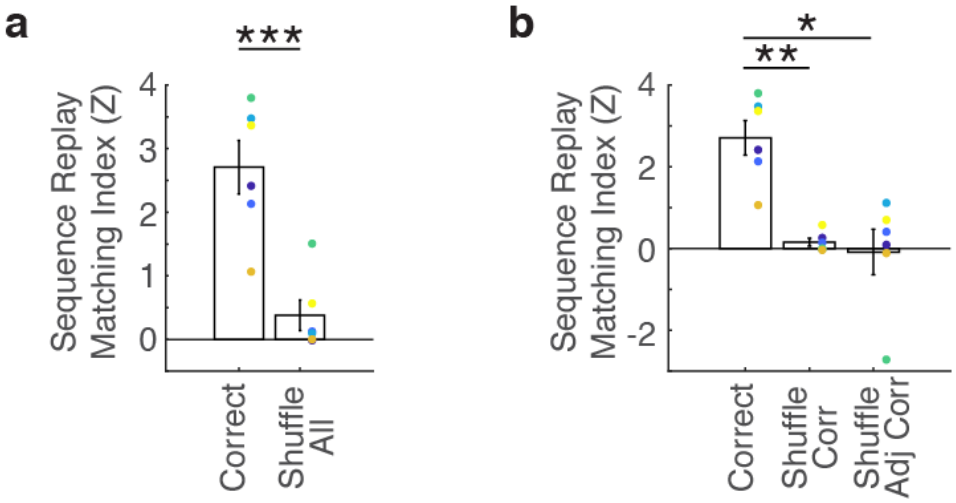

Replication of memory specificity results using single sequences from encoding and retrieval. To test if memory specificity was present at the level of single sequences, we selected single sequences from each encoding-retrieval trial pair and performed a similar shuffling procedure as described in Fig. 3e,f. We hypothesized that individual sequences would contain memory specific information. In each trial, we therefore selected the encoding-retrieval sequence pair that exhibited the highest replay value (matching index). In the case that more than one sequence pair exhibited the same matching index, we selected one of these pairs at random. We computed z-scores of the resulting MI calculations based on the original distribution for comparison purposes. **a**, Sequence replay for true encoding-retrieval comparisons was significantly greater than replay calculated after shuffling encoding labels for all trials (n = 6, paired t-test, $t(5) = 7.31$, $p < 0.001$). Each colored dot represents a replay value for one participant and bars indicate SEM across all participants. **b**, Sequence replay for correct trials versus shuffled correct trial conditions. True encoding-retrieval pairs were significantly more similar than shuffled correct and shuffled adjacent correct trials (one-way ANOVA across all categories: $F(2) = 14.51$, $p < 0.001$; post-hoc paired t-test for each category pair, $^{**}p < 0.01$, $^{*}p < 0.05$)

Fig. S19

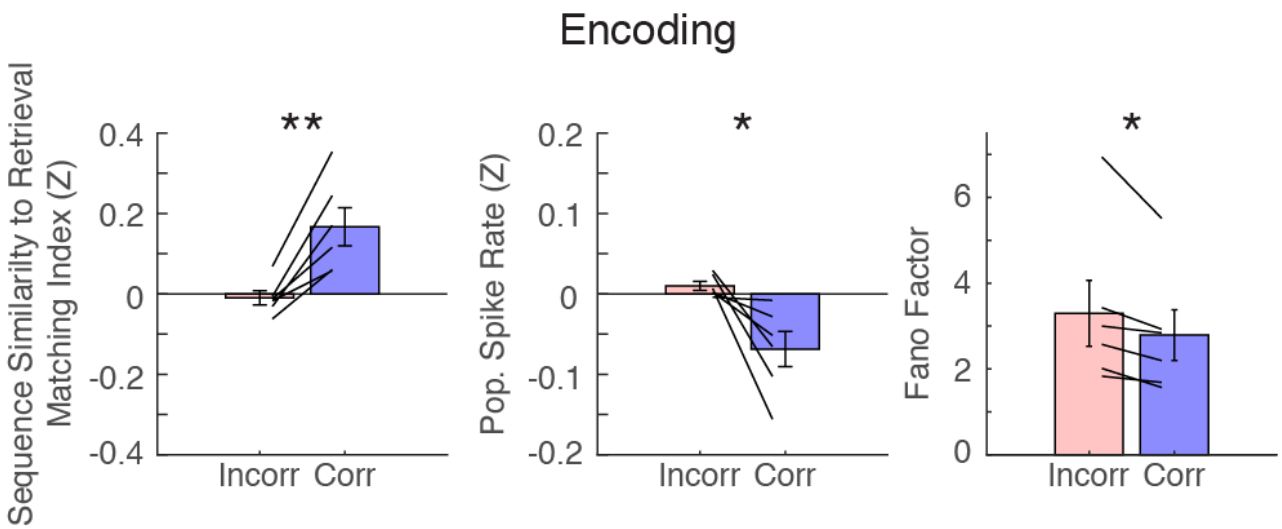

Spiking characteristics during encoding mirror those during retrieval. Increased sequence similarity between encoding burst events and retrieval events (left; n = 6, t(5) = 5.30, p = .003) was accompanied by decreased population spike rate (middle; t(5) = -4.59, p = .006) and decreased Fano factor (right; t(5) = -2.63, p = .046) during encoding. Each line indicates a single participant and bars indicate SEM across all participants. (*$p < 0.05$, **$p < 0.01$).

Fig. S20

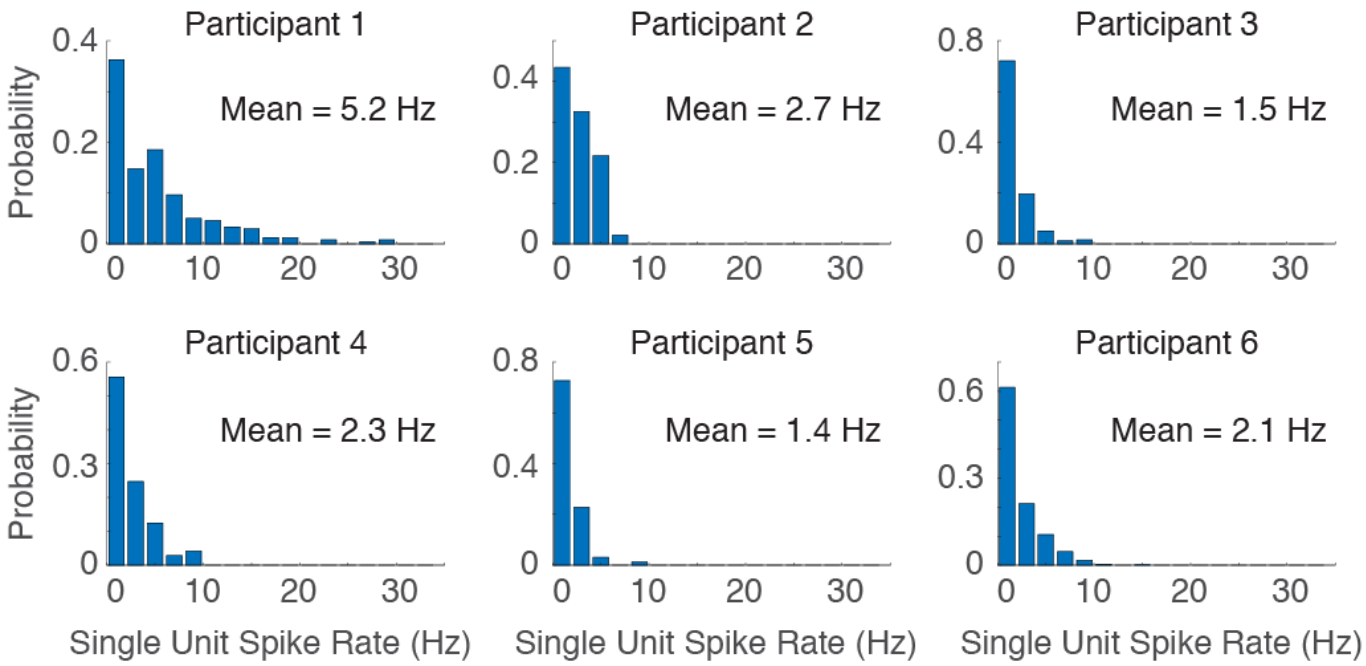

Individual participant distributions of single unit spike rates. Values represent the average spike rate of each single unit, and the average rate for each participant is shown in the inset text. Average spike rate across all participants is 2.5 ± 0.6 Hz.

Fig. S21

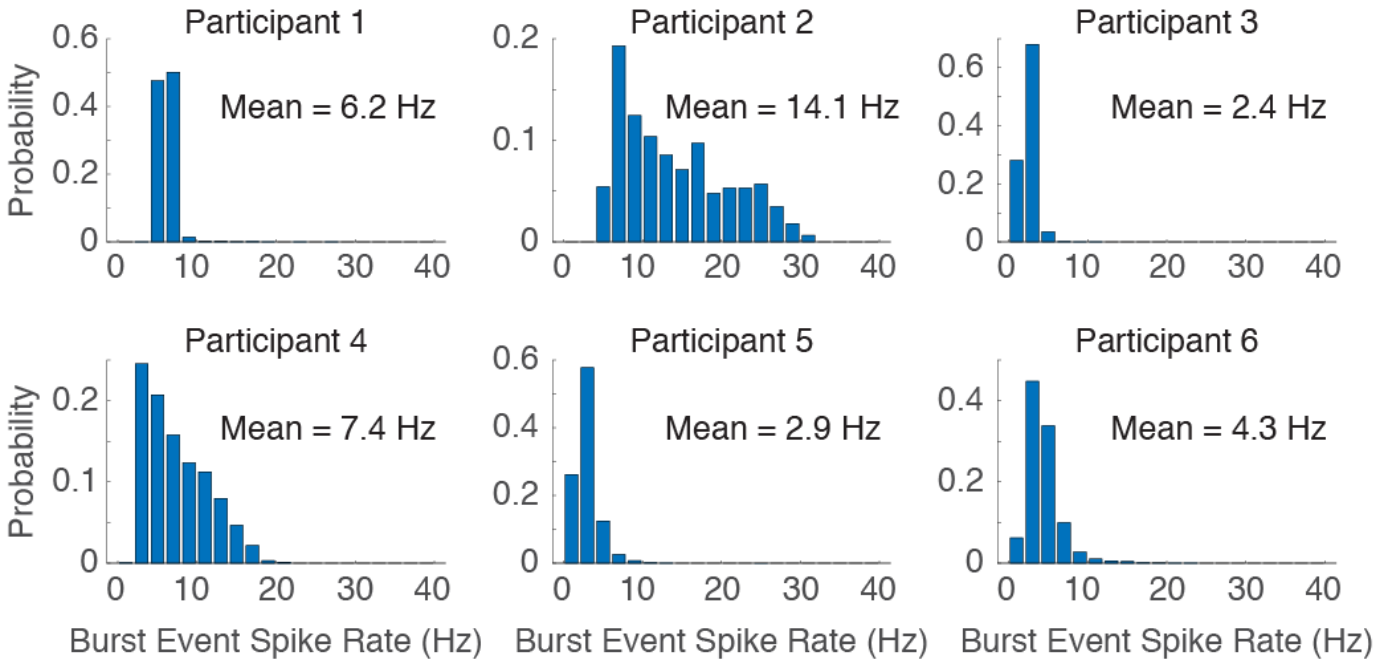

Individual participant distributions of burst event spike rates. Values represent the average spike rate of all units during each burst event, and the average rate for each participant is shown in the inset text. Average burst event spike rate across all participants is 6.2 ± 1.8 Hz.

Fig. S22

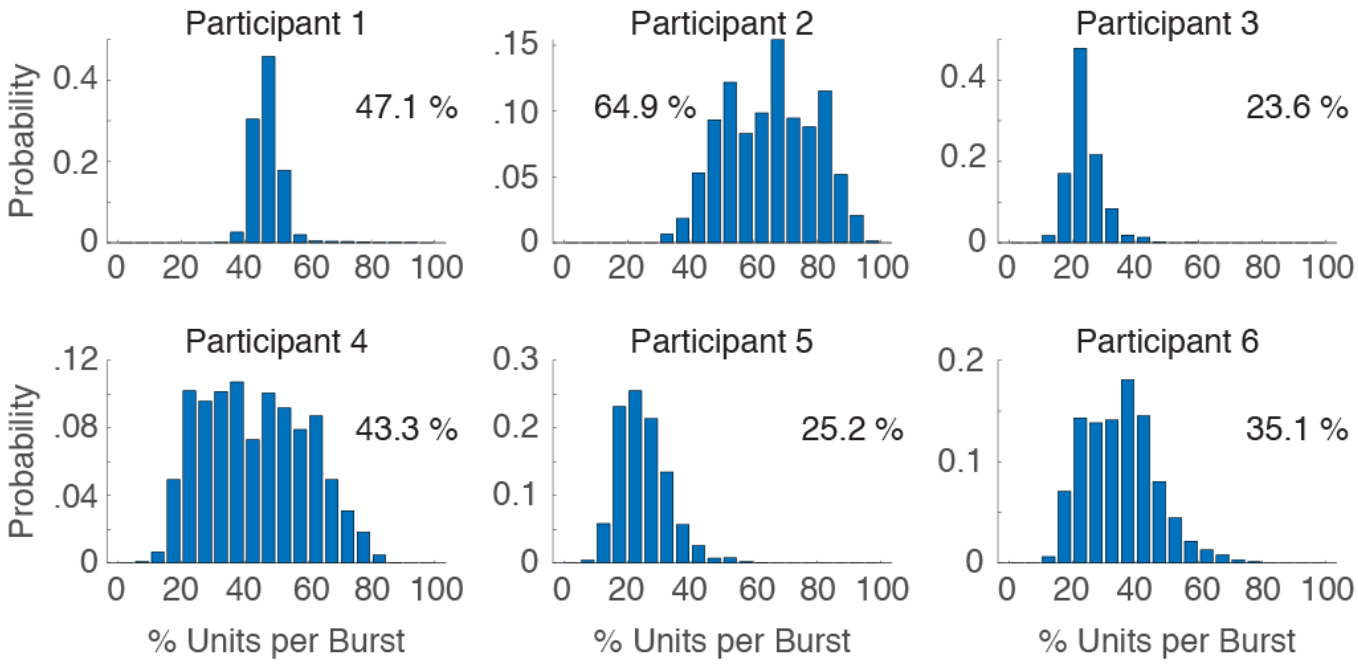

Individual participant distributions of percentage of units active per burst event. Values represent the percentage of units active during each burst event (at least one spike), and the average for each participant is shown in the inset text. Average percentage across all participants is 39.9 ± 6.3 %.

Fig. S23

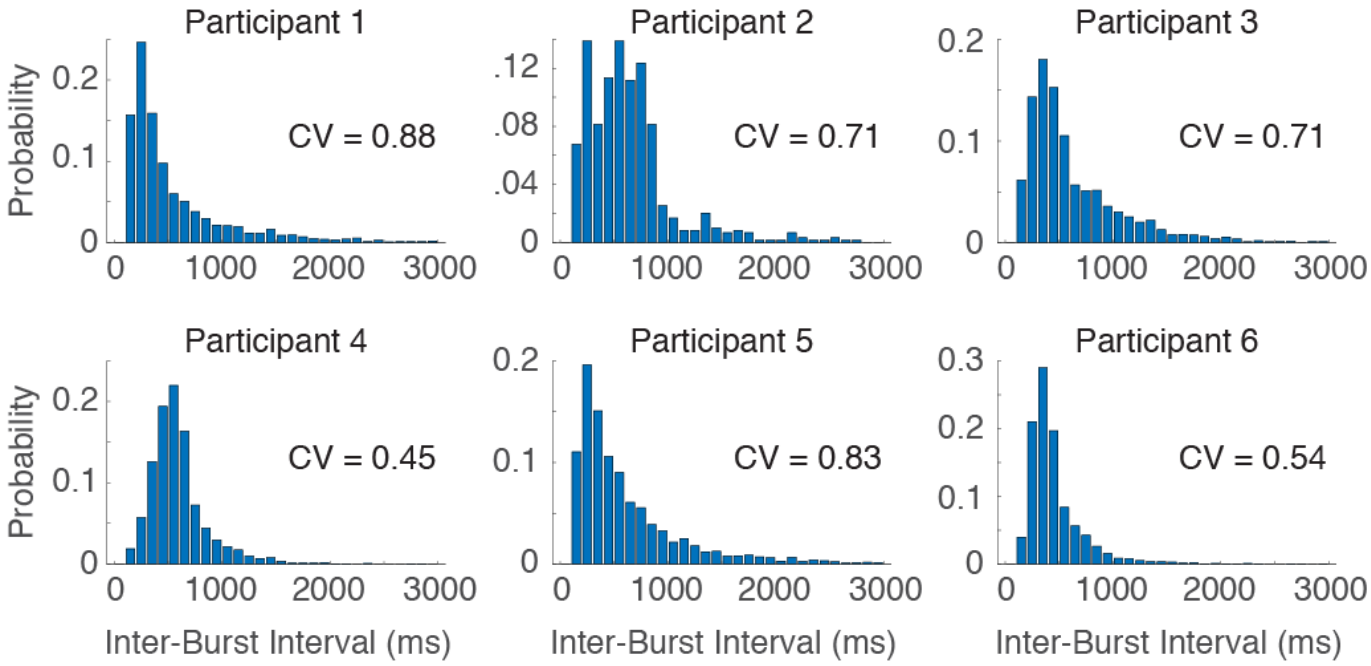

Individual participant distributions of inter-burst intervals. Values represent the inter-event intervals for burst events, and the coefficient of variation (CV) for each participant is shown in the inset text. Average CV across all participants is 0.69 ± 0.07 and average inter-burst interval is 579 ± 71 ms.

Fig. S24

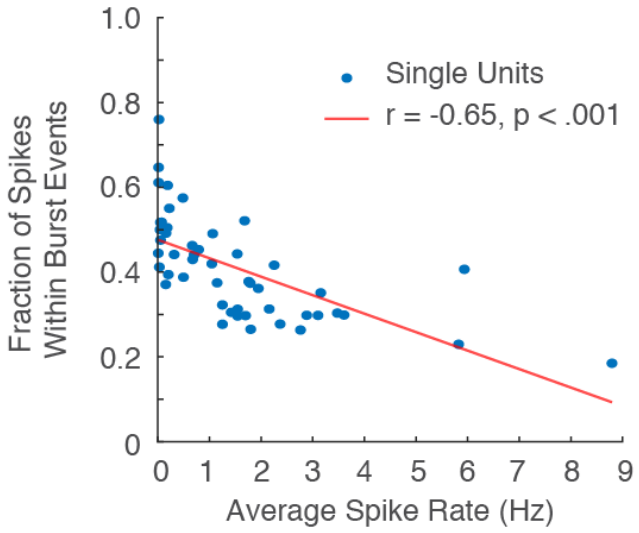

Units with lower spike rates are more selective for firing within burst events. Example session is shown where the average spike rate of each unit is plotted against its fraction of spikes within burst events. Each blue point is a single unit within that session, and the red line indicates the linear regression through all points. Across all participants, the average spike rate and fraction of spikes within burst events were inversely correlated ($r = -0.35 \pm 0.06$, $t(5) = -5.60$, $p = .003$).

Fig. S25

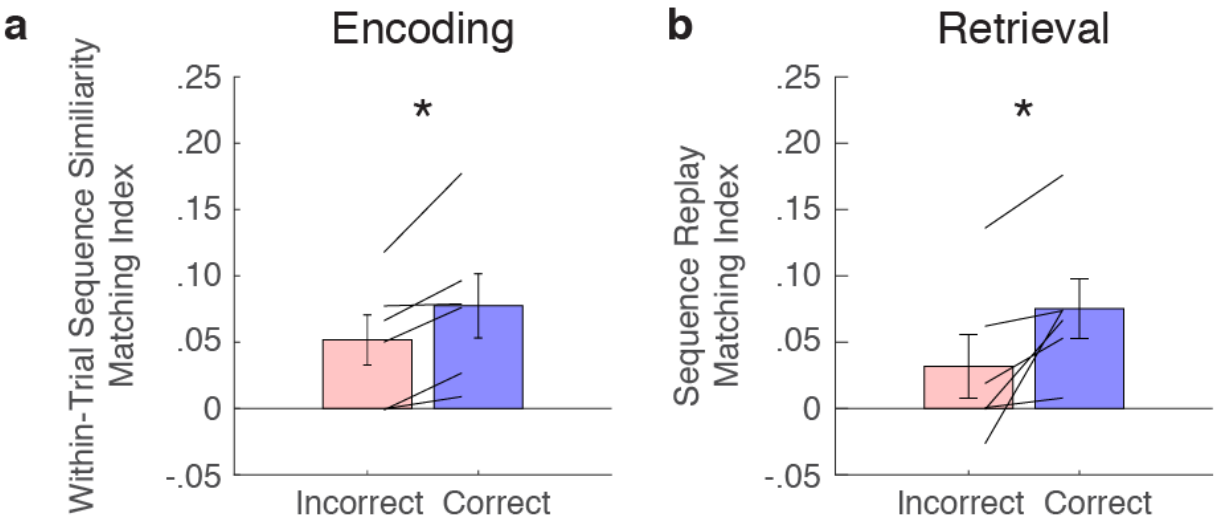

Replication of main results with raw MI values. a, Encoding sequences in correct trials demonstrated higher within-trial similarity than in incorrect trials (compare to Fig. 2e; n = 6, t(5) = 3.14, p = 0.026; *p < 0.05). **b**, Sequence replay was higher in correct trials compared to incorrect trials (compare to Fig. 3g; t(5) = 3.01, p = 0.030).

Fig. S26

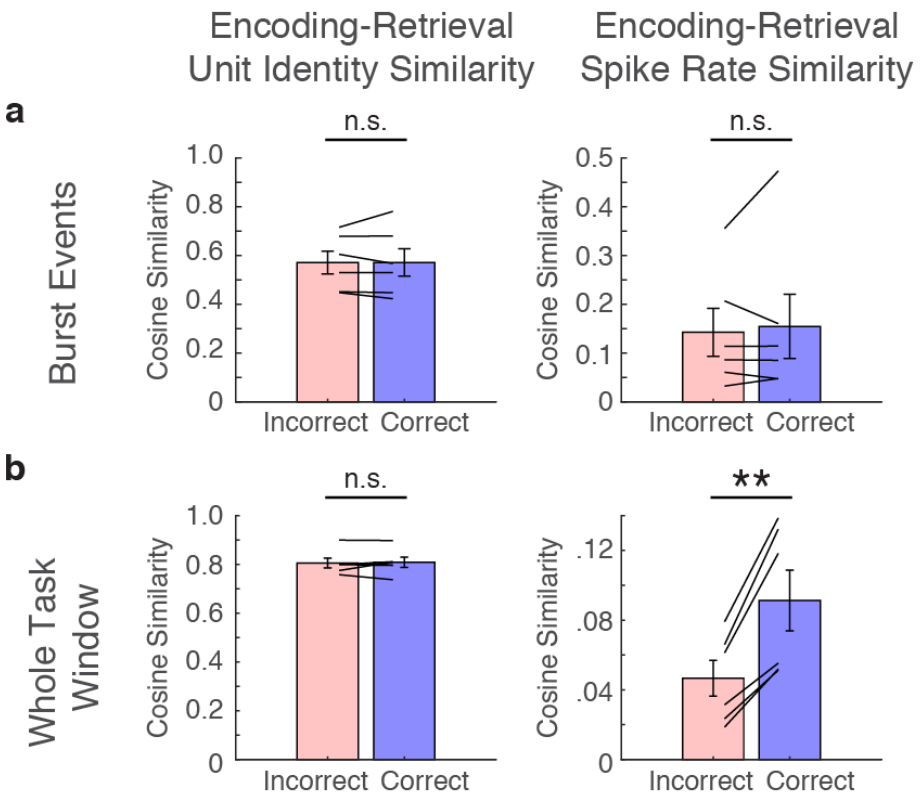

Increases in spike rate similarity between correct encoding and retrieval are measurable when analyzing the whole task window as opposed to individual burst events. Because we found no significant difference in the similarity of unit identity between encoding and retrieval when comparing correct to incorrect trials, we were interested in whether the similarity of z-scored spike rates for each unit differed between trial types. We quantified the extent to which the pattern of z-scored spiking rates across all units were similar between encoding and retrieval in each trial (*27*). **a**, Within burst events, we observed no significant difference between encoding-retrieval unit identity similarity (left) or in spike rate similarity (right) when comparing correct to incorrect trials. **b**, When we averaged across the whole task window (0 to 4 s after study pair presentation and -1 to 0 s before retrieval), however, we found that although unit identity was again not significantly different between trial types (left), spike rate similarity was significantly different between correct and incorrect trials (right; $t(5) = 5.95$, $p = .002$; $^{**}p < 0.01$). These results suggest that the reinstatement of patterns of spiking activity observed between correct encoding and retrieval and reported in previous analyses (*27*) is driven by the patterns of memory-specific decreases in spiking activity that are present across the population of units across many burst events. Within individual burst events, however, the temporal order of those active neurons rather than their identity or absolute rate drive the observed similarity between correct encoding and retrieval.

Fig. S27

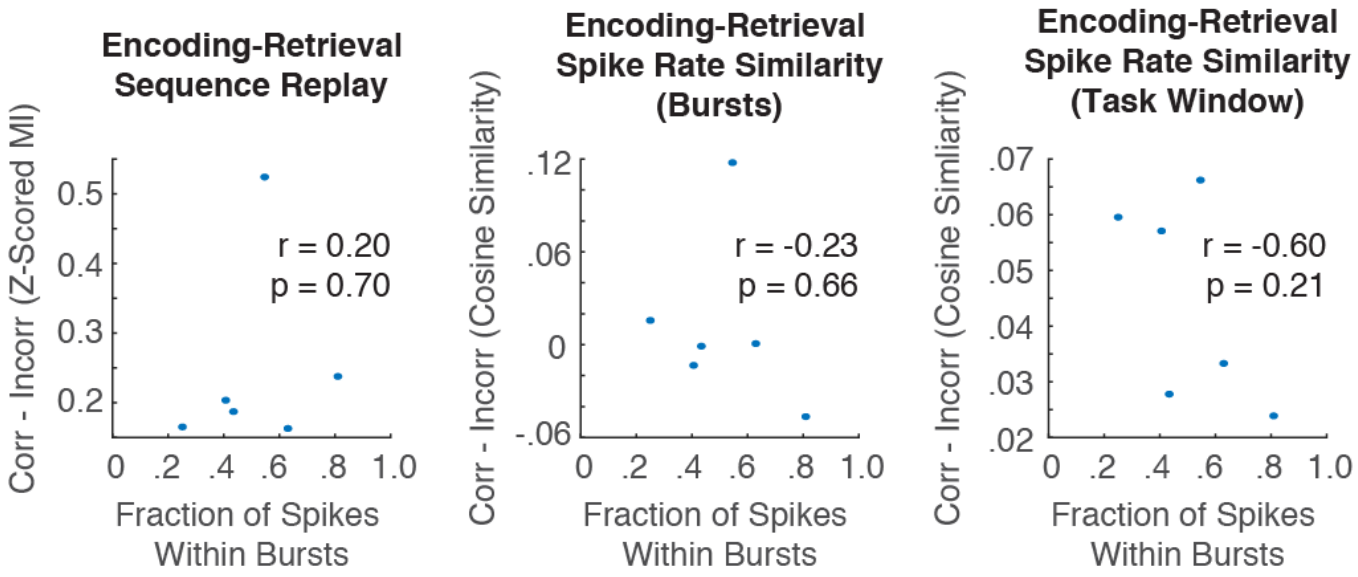

Sequence replay and spike rate similarity between encoding and retrieval are not correlated with fraction of spikes within burst events. Because the apparent burstiness of the spike rasters varied significantly across participants, we quantified the average fraction of spikes within burst events across all units for each participant (average of 0.51 ± 0.08 across participants). We found no significant correlation between the fraction of spikes within burst events and sequence replay values (left), encoding-retrieval spike rate similarity within burst events, or encoding-retrieval spike rate similarity across the whole task window. Each blue point represents the average values for each participant. Pearson correlation values and associated p-values are shown in each inset.

Supplementary Table S1

Participant	Age	Sex	Language Dominance	Seizure Focus	Resection	Microelectrode Array Implantation
1	28	M	L	L temporal	None	L ATL (STG)
2	39	M	L	R temporal	R temporal lobectomy w/ amygdalohippocampectomy	R ATL (MTG)
3	51	M	L	L temporal	L selective amygdalohippocampectomy	L ATL (MTG)
4	43	F	L	L temporal	L temporal lobectomy w/ amygdalohippocampectomy	L ATL (MTG)
5	28	F	L	L temporal	L temporal lobectomy w/ amygdalohippocampectomy	L ATL (MTG)
6	20	M	L	L temporal	L superior temporal corticectomy	L ATL (MTG)

ATL = Anterior Temporal Lobe
STG = Superior Temporal Gyrus
MTG = Middle Temporal Gyrus

Supplementary Discussion

The general interpretation of the emergence and functional importance of neural sequences derives heavily from the place cell literature, where the replay of these sequences has been implicated as a neural substrate of learning and memory (*7–14*). The actual content of these sequences is composed of transitions between neural populations that represent discrete locations in space. However, this general motif of representing information with sequences can also abstract beyond spatial representations (*34*). As such, it has been proposed that neural sequences bind sequentially experienced sensory input into a content-free, down-sampled representation within the hippocampus (*35*). This manner of organization of episodic memory allows for expedient and efficient access to the relevant sensory experiences that are distributed across cortical modules for purposes of memory retrieval or consolidation.

Extending this conceptual framework to our data, sequences may arise in the paired-associates task via one of two interpretations. The first possible interpretation is concordant with the place cell literature in that sequences could be observed due to a temporally ordered transition between the neural populations that encode discrete concepts. For example, in our data, the measured sequences associated with the word pair “CROW JEEP” could represent a transition between the neural populations for “CROW” and “JEEP” respectively. Indeed this interpretation is consistent with previous evidence from paired-associates tasks in the non-human primate literature (*36*, *37*).

However, the second interpretation regarding the emergence of sequences in our data is that individual abstract concepts are encoded by sequences in the human brain. Within this interpretation, the novel association between two unrelated words is represented neurally by a sequence of spiking activity, independent of a transition between the respective neural populations. That is, the abstraction “CROW JEEP” is represented neurally by a sequence irrespective of the network organizations that respectively encode “CROW” or “JEEP”. We believe that this interpretation is more likely in our data given that participants often use mnemonic strategies of imagining abstract concepts to remember word pairs. Additionally, if sequences represent transitions between the respective words in a pair, the order of presentation of words should influence sequence trajectory (eg. “CROW JEEP” or “JEEP CROW”). However, our task design involved randomly choosing the first or second word to use as a test probe during memory retrieval, and no difference in sequence replay was observed between the two cases. Taken together, this interpretation implies that the temporal ordering of neurons is intrinsically important for the representation of individual concepts in the brain, in addition to capturing the temporal order of experience in episodic memory as is observed with rodent place cells. Future studies can further disambiguate these two cases by potentially observing the emergence of sequences for memory of single discrete concepts, such as in free-recall paradigms with lists of single nouns.

As for more general coding mechanisms within the brain, we observed two distinct potential mechanisms for information representation in our data. We show that the fine grained temporal ordering of neural spiking activity within burst events during retrieval recapitulates the memory-specific ordering from encoding. However, we also observed decreases in spike rates over the whole task window during both encoding and retrieval, and these changes were consistent with memory-specific spike rate reinstatement during memory retrieval (*27*). These results suggest then that a spiking network could store information over larger timescales with gross changes in spike rates while also implementing a temporal ordering code at smaller timescales. This duality of motifs for information coding could be relevant for forming and maintaining dynamic memory representations at different neural and behavioral timescales.

References and Notes

1. E. Tulving, in *Organization of Memory*, E. Tulving, W. Donaldson, Eds. (Academic Press, 1972), pp. 381–403.

2. J. L. McClelland, B. L. McNaughton, R. C. O'Reilly, Why there are complementary learning systems in the hippocampus and neocortex: Insights from the successes and failures of connectionist models of learning and memory. *Psychol. Rev.* **102**, 419–457 (1995). doi:10.1037/0033-295X.102.3.419 Medline

3. J. D. Johnson, M. D. Rugg, Recollection and the reinstatement of encoding-related cortical activity. *Cereb. Cortex* **17**, 2507–2515 (2007). doi:10.1093/cercor/bhl156 Medline

4. B. P. Staresina, R. N. A. Henson, N. Kriegeskorte, A. Alink, Episodic reinstatement in the medial temporal lobe. *J. Neurosci.* **32**, 18150–18156 (2012). doi:10.1523/JNEUROSCI.4156-12.2012 Medline

5. L. Deuker, J. Olligs, J. Fell, T. A. Kranz, F. Mormann, C. Montag, M. Reuter, C. E. Elger, N. Axmacher, Memory consolidation by replay of stimulus-specific neural activity. *J. Neurosci.* **33**, 19373–19383 (2013). doi:10.1523/JNEUROSCI.0414-13.2013 Medline

6. R. B. Yaffe, M. S. D. Kerr, S. Damera, S. V. Sarma, S. K. Inati, K. A. Zaghloul, Reinstatement of distributed cortical oscillations occurs with precise spatiotemporal dynamics during successful memory retrieval. *Proc. Natl. Acad. Sci. U.S.A.* **111**, 18727–18732 (2014). doi:10.1073/pnas.1417017112 Medline

7. W. E. Skaggs, B. L. McNaughton, Replay of neuronal firing sequences in rat hippocampus during sleep following spatial experience. *Science* **271**, 1870–1873 (1996). doi:10.1126/science.271.5257.1870 Medline

8. Z. Nádasdy, H. Hirase, A. Czurkó, J. Csicsvari, G. Buzsáki, Replay and time compression of recurring spike sequences in the hippocampus. *J. Neurosci.* **19**, 9497–9507 (1999). doi:10.1523/JNEUROSCI.19-21-09497.1999 Medline

9. A. K. Lee, M. A. Wilson, Memory of sequential experience in the hippocampus during slow wave sleep. *Neuron* **36**, 1183–1194 (2002). doi:10.1016/S0896-6273(02)01096-6 Medline

10. D. J. Foster, M. A. Wilson, Reverse replay of behavioural sequences in hippocampal place cells during the awake state. *Nature* **440**, 680–683 (2006). doi:10.1038/nature04587 Medline

11. K. Diba, G. Buzsáki, Forward and reverse hippocampal place-cell sequences during ripples. *Nat. Neurosci.* **10**, 1241–1242 (2007). doi:10.1038/nn1961 Medline

12. D. Ji, M. A. Wilson, Coordinated memory replay in the visual cortex and hippocampus during sleep. *Nat. Neurosci.* **10**, 100–107 (2007). doi:10.1038/nn1825 Medline

13. M. F. Carr, S. P. Jadhav, L. M. Frank, Hippocampal replay in the awake state: A potential substrate for memory consolidation and retrieval. *Nat. Neurosci.* **14**, 147–153 (2011). doi:10.1038/nn.2732 Medline

14. B. E. Pfeiffer, D. J. Foster, Hippocampal place-cell sequences depict future paths to remembered goals. *Nature* **497**, 74–79 (2013). doi:10.1038/nature12112 Medline

15. G. Girardeau, K. Benchenane, S. I. Wiener, G. Buzsáki, M. B. Zugaro, Selective suppression of hippocampal ripples impairs spatial memory. *Nat. Neurosci.* **12**, 1222–1223 (2009). doi:10.1038/nn.2384 Medline

16. S. P. Jadhav, C. Kemere, P. W. German, L. M. Frank, Awake hippocampal sharp-wave ripples support spatial memory. *Science* **336**, 1454–1458 (2012). doi:10.1126/science.1217230 Medline

17. G. Buzsáki, Hippocampal sharp wave-ripple: A cognitive biomarker for episodic memory and planning. *Hippocampus* **25**, 1073–1188 (2015). doi:10.1002/hipo.22488 Medline

18. D. Khodagholy, J. N. Gelinas, G. Buzsáki, Learning-enhanced coupling between ripple oscillations in association cortices and hippocampus. *Science* **358**, 369–372 (2017). doi:10.1126/science.aan6203 Medline

19. H. R. Joo, L. M. Frank, The hippocampal sharp wave-ripple in memory retrieval for immediate use and consolidation. *Nat. Rev. Neurosci.* **19**, 744–757 (2018). doi:10.1038/s41583-018-0077-1 Medline

20. A. Fernández-Ruiz, A. Oliva, E. Fermino de Oliveira, F. Rocha-Almeida, D. Tingley, G. Buzsáki, Long-duration hippocampal sharp wave ripples improve memory. *Science* **364**, 1082–1086 (2019). doi:10.1126/science.aax0758 Medline

21. N. Axmacher, C. E. Elger, J. Fell, Ripples in the medial temporal lobe are relevant for human memory consolidation. *Brain* **131**, 1806–1817 (2008). doi:10.1093/brain/awn103 Medline

22. B. P. Staresina, T. O. Bergmann, M. Bonnefond, R. van der Meij, O. Jensen, L. Deuker, C. E. Elger, N. Axmacher, J. Fell, Hierarchical nesting of slow oscillations, spindles and ripples in the human hippocampus during sleep. *Nat. Neurosci.* **18**, 1679–1686 (2015). doi:10.1038/nn.4119 Medline

23. H. Zhang, J. Fell, N. Axmacher, Electrophysiological mechanisms of human memory consolidation. *Nat. Commun.* **9**, 4103 (2018). doi:10.1038/s41467-018-06553-y Medline

24. Y. Liu, R. J. Dolan, Z. Kurth-Nelson, T. E. J. Behrens, Human replay spontaneously reorganizes experience. *Cell* **178**, 640–652.e14 (2019). doi:10.1016/j.cell.2019.06.012 Medline

25. A. P. Vaz, S. K. Inati, N. Brunel, K. A. Zaghloul, Coupled ripple oscillations between the medial temporal lobe and neocortex retrieve human memory. *Science* **363**, 975–978 (2019). doi:10.1126/science.aau8956 Medline

26. T. M. Norman, M. A. Horlbeck, J. M. Replogle, A. Y. Ge, A. Xu, M. Jost, L. A. Gilbert, J. S. Weissman, Exploring genetic interaction manifolds constructed from rich single-cell phenotypes. *Science* **365**, eaax1030 (2019). doi:10.1126/science.aax4438 Medline

27. A. I. Jang, J. H. Wittig Jr., S. K. Inati, K. A. Zaghloul, Human cortical neurons in the anterior temporal lobe reinstate spiking activity during verbal memory retrieval. *Curr. Biol.* **27**, 1700–1705.e5 (2017). doi:10.1016/j.cub.2017.05.014 Medline

28. J. H. Wittig Jr., A. I. Jang, J. B. Cocjin, S. K. Inati, K. A. Zaghloul, Attention improves memory by suppressing spiking-neuron activity in the human anterior temporal lobe. *Nat. Neurosci.* **21**, 808–810 (2018). doi:10.1038/s41593-018-0148-7 Medline

29. M. Le Van Quyen, A. Bragin, R. Staba, B. Crépon, C. L. Wilson, J. Engel Jr., Cell type-specific firing during ripple oscillations in the hippocampal formation of humans. *J. Neurosci.* **28**, 6104–6110 (2008). doi:10.1523/JNEUROSCI.0437-08.2008 Medline

30. G. Buzsáki, Two-stage model of memory trace formation: A role for "noisy" brain states. *Neuroscience* **31**, 551–570 (1989). doi:10.1016/0306-4522(89)90423-5 Medline

31. M. S. Trotta, J. Cocjin, E. Whitehead, S. Damera, J. H. Wittig Jr., Z. S. Saad, S. K. Inati, K. A. Zaghloul, Surface based electrode localization and standardized regions of interest for intracranial EEG. *Hum. Brain Mapp.* **39**, 709–721 (2018). doi:10.1002/hbm.23876 Medline

32. M. R. Cohen, J. H. R. Maunsell, Attention improves performance primarily by reducing interneuronal correlations. *Nat. Neurosci.* **12**, 1594–1600 (2009). doi:10.1038/nn.2439 Medline

33. E. Maris, R. Oostenveld, Nonparametric statistical testing of EEG- and MEG-data. *J. Neurosci. Methods* **164**, 177–190 (2007). doi:10.1016/j.jneumeth.2007.03.024 Medline

34. D. Aronov, R. Nevers, D. W. Tank, Mapping of a non-spatial dimension by the hippocampal-entorhinal circuit. *Nature* **543**, 719–722 (2017). doi:10.1038/nature21692 Medline

35. G. Buzsáki, D. Tingley, Space and time: The hippocampus as a sequence generator. *Trends Cogn. Sci.* **22**, 853–869 (2018). doi:10.1016/j.tics.2018.07.006 Medline

36. K. Sakai, Y. Miyashita, Neural organization for the long-term memory of paired associates. *Nature* **354**, 152–155 (1991). doi:10.1038/354152a0 Medline

37. Y. Naya, K. Sakai, Y. Miyashita, Activity of primate inferotemporal neurons related to a sought target in pair-association task. *Proc. Natl. Acad. Sci. U.S.A.* **93**, 2664–2669 (1996). doi:10.1073/pnas.93.7.2664 Medline